2005

FABRICATION AND CHARACTERIZATION OF CuPc BASED ORGANIC SOLAR CELLS

Balaji Parthasarathy
University of Kentucky, balaji@engr.uky.edu

ABSTRACT OF THESIS

FABRICATION AND CHARACTERIZATION OF CuPc BASED ORGANIC SOLAR CELLS

In this work, organic solar cells of the configuration ITO/Pedot:PSS/CuPc/PTCBI/Al (Indium tin oxide/poly(3,4-ethylenedioxythiophene): polystyrene sulfonic acid/copper phthalocyanine/3,4,9,10-perylenetetracarboxylic bisbenzimidazole/aluminum) were investigated. A high open-circuit voltage (V_{oc}) of 1.15 V was obtained when the PTCBI layer was 7 nm thick. Lower V_{oc} values were observed for the same structure with silver, copper and gold electrodes instead of aluminum. However, short-circuit current density (J_{sc}) with these electrodes was much higher (4 mA/cm^2) than in the case of aluminum (0.12 mA/cm^2). Results were interpreted in terms of a modified CuPc/Al Schottky diode for the thin PTCBI case and a CuPc/PTCBI heterojunction for the thick PTCBI case. Also, the formation of a thin, protective aluminum oxide layer under the aluminum electrode was postulated. For devices with silver, copper and gold electrodes, absence of this protective layer was thought to be the cause of a relatively lower V_{oc} and higher J_{sc}.

KEYWORDS: CuPc/PTCBI solar cells, organic semiconductors, excitons, modified Schottky diode.

Balaji Parthasarathy

November 7th, 2005

FABRICATION AND CHARACTERIZATION OF CuPc BASED ORGANIC SOLAR CELLS

By

Balaji Parthasarathy

Dr. Vijay P. Singh
(Director of Thesis)

Dr, YuMing Zhang
(Director of Graduate Studies)

November 7th, 2005

FABRICATION AND CHARACTERIZATION OF CuPc BASED ORGANIC SOLAR CELLS

By

Balaji Parthasarathy

Dr. Arthur V. Radun
(Co-Director of Thesis)

Dr. Janet K. Lumpp
(Co-Director of Thesis)

Dr, YuMing Zhang
(Director of Graduate Studies)

November 7th, 2005

RULES FOR THE USE OF THESES

Unpublished theses submitted for the Master's degree and deposited in the University of Kentucky Library are as a rule open for inspection, but are to be used only with due regard to the rights of the authors. Bibliographical references may be noted, but quotations or summaries of parts may be published only with the permission of the author, and with the usual scholarly acknowledgements.

Extensive copying or publication of the thesis in whole or in part also requires the consent of the Dean of the Graduate School of the University of Kentucky.

A library that borrows this thesis for use by its patrons is expected to secure the signature of each user.

Name	Date

THESIS

FABRICATION AND CHARACTERIZATION OF CuPc BASED ORGANIC SOLAR CELLS

By

Balaji Parthasarathy

The Graduate School

University of Kentucky

2005

FABRICATION AND CHARACTERIZATION OF CuPc BASED ORGANIC SOLAR CELLS

THESIS

A thesis submitted in partial fulfillment of the requirements for the degree of Master of Science in the College of Engineering
at the University of Kentucky

By

Balaji Parthasarathy

Lexington, Kentucky

Director: Dr. Vijay P. Singh, Professor of Electrical Engineering

Lexington, Kentucky

2005

MASTER'S THESIS RELEASE

I authorize the University of Kentucky
Libraries to reproduce this thesis in
whole or in part for purposes of research.

Signed: Balaji Parthasarathy
Date: November 7th, 2005

ACKNOWLEDGEMENTS

I sincerely thank Dr. Vijay P. Singh for providing me the opportunity to work in the field of organic solar cells and also for his invaluable guidance and encouragement throughout this research work. Next, I wish to thank Dr. Arthur V. Radun and Dr. Janet K. Lumpp for serving on my thesis committee and providing helpful comments for the improvement of this report. I would also like to thank Dr. John Anthony and Marcia Payne for their help in the preparation of organic chemicals used in this work.

I sincerely thank Dr. Suresh S. Rajaputra for his constant support and guidance throughout the course of this work. I would also like to acknowledge and thank Dr. Alberto Aguilera for his contribution towards this work. I also thank all the student members of the Electronic Devices Research Group for creating an amicable atmosphere in the lab.

Finally, I express my gratitude and thanks to my parents and family for all the support they offered to help me stay motivated and successfully complete this work.

TABLE OF CONTENTS

List of Tables

List of Figures

List of Files

Chapter 1. Introduction

Molecular electronic materials such as small molecule films and conjugated polymers are of interest in photovoltaic applications [1-4] due to their ease of fabrication and compatibility with flexible substrates, thus offering the prospect of low-cost solar cell production. This emerging field of organic semiconductor materials and devices has made impressive progress in recent years, extending the capabilities and possibilities of modern electronic and photonic devices into unexpected domains [2]. However, organic semiconductors continue to suffer from low photocurrents and low fill factors [4]. Also, the device behavior is not as well understood as in the case of inorganic solar cells [5-8] and thereby necessitating a need for further research in this area.

This work aims at the selection of suitable organic semiconductors and metal electrodes and in optimizing their fabrication processes in order to achieve high photovoltage. From the rich variety of organic semiconductors, phthalocyanines (Pcs) have been extensively used in experimental optoelectronic devices, with CuPc/PTCBI (copper phthalocyanine/3,4,9,10-perylenetetracarboxylic bisbenzimidazole) proven to being a promising heterojunction for organic photovoltaics [4]. Under AM2 illumination, Tang et al. achieved an open circuit voltage (V_{oc}) of 450 mV and a short circuit current density (J_{sc}) of 2.3 mA/cm^2 using this structure [1]. Later, Forrest et al reported a V_{oc} of 0.48 V and J_{sc} of 4.2 mA/cm^2 using this structure but with a silver electrode [9]. In this work we primarily report the fabrication and characterization of single junction CuPc/PTCBI devices that exhibit a V_{oc} of 1.15 V and J_{sc} of 0.125 mA/cm^2. With a view toward attaining higher short circuit current density, several modifications to this basic design structure were also studied.

Chapter 2. Theory

2.1. Principle of organic solar cells

Organic solar cells differ from their inorganic counterparts in the process by which free charge carriers are created upon optical absorption. One of the main differences between organic and inorganic solar cells is that the absorption of light in the organic semiconductors does not directly lead to the generation of free charge carriers, instead the absorption of a photon by a molecule results in the formation of a molecular exciton. The exciton can be described as a bound electron-hole pair with a binding energy of about 0.4 eV [10-12].

Thus upon optical excitation of an organic material, localized Frenkel or charge-transfer excitons are generated [2]. These excitons need to be split up (or dissociated) before the charges can be transported through the organic films and collected at the respective electrodes. For example, exciton dissociation can occur at a rectifying interface (Schottky contact) in single layer devices or at the interface between an electron-donor and an electron-acceptor semiconductor material. The larger this interface area the more excitons can reach it and dissociate into free charges [13]. To obtain a high photosensitivity, exciton dissociation at a donor-acceptor interface must be preceded by efficient transport of the photogenerated excitons toward this interface, and followed by efficient charge extraction at low bias. Complete transport of excitons to the donor-acceptor interface is achieved by establishing an intimate contact between the donor and acceptor materials by means of implementing various design techniques such as blending, laminating, codeposition or chemical linking [2].

2.2. Dissociation of excitons

As mentioned earlier, in organic semiconductors, absorption of photons leads to the creation of bound electron hole pairs (excitons) rather than free charges. These excitons carrying energy but no net charge may diffuse to dissociation sites where their charges can be separated. The separated charges then need to travel to the respective device electrodes, holes to the anode and electrodes to the cathode to provide voltage and be available for injection into an external circuit.

Photogenerated excitons are strongly bound and do not spontaneously dissociate into charge pairs [14]. Dissociation of excitons requires an input energy of 100 meV compared to a few meV needed for a crystalline semiconductor. Typically in-built electric fields created by the work function difference between the donor and acceptor materials are seldom sufficient to break up the photogenerated excitons. Instead, the exciton diffuses within the organic layers until it reaches a contact where it may be broken up to supply separate free charges. Another mechanism by which photogenerated excitons dissociate into free charges is by traveling to the donor-acceptor interface in a heterojunction device. At the interface between two different materials, electrostatic forces result from the differences in their electron affinity and ionization potential. If both electron affinity and ionization potential are greater in one material (electron acceptor) than the other (electron donor) then the interfacial electric field drives the charge separation. These local electric fields will succeed in breaking up the photogenerated excitons provided that the differences in potential energies are larger than the exciton binding energy. If the distance that an exciton has to travel in order to reach a donor-acceptor interface to dissociate is smaller than the exciton diffusion length of that material, then whenever an exciton is photogenerated in either material, it is likely to diffuse to an

interface and break up. If continuous paths exist in each material from the interface to the respective electrodes, then the separated charge carriers may travel to the contacts and deliver current to the external circuit. This process [14] is illustrated in Figure 2.1 where an exciton dissociates near a donor-acceptor interface.

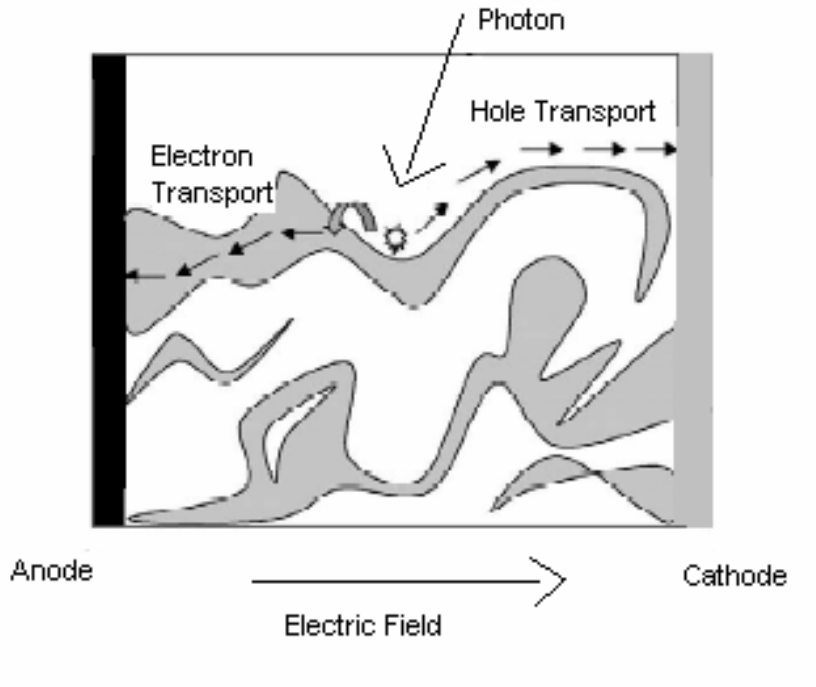

Figure 2.1: Dissociation of excitons at a donor-acceptor interface

2.3. Organic semiconductors

Organic electronic materials are conjugated solids where both optical absorption and charge transport are dominated by partly delocalized л and л * orbitals [14]. Candidates for photovoltaic applications include crystalline or polycrystalline films of small molecules, amorphous films of small molecules prepared by vacuum deposition or solution processing, films of conjugated polymers or oligomers processed from solution, and combinations of any of these either with other organic solids or with inorganic materials. Efficient organic donor-acceptor interfaces can be achieved by implementing various processing techniques such as blending, laminating, codeposition or chemical linking. Further current harvesting in organic devices can be optimized by employing exciton-blocking layers and implementing stacked architectures. In stacked architectures several numbers of layers are stacked on top of each other in a multilayer configuration. Reflections at interfaces affect the distribution of the optical electric field inside these thin film photodiodes.

In spite of such flexibilities in their processing methods, organic semiconductors do come with some disadvantages such as requiring a strong driving force such as an electric field to be present to break up the photogenerated excitons, limiting the useful device thicknesses due to their low charge carrier mobilities and their sensitivities to temperature.

2.4. Organic solar cell architectures

In order to achieve efficient exciton dissociation the organic solar cell should have sufficient interface sites for the excitons to reach and break into free charge carriers. This could be achieved by increasing the donor-acceptor interface area and also the donor-anode and acceptor-cathode interface sites. Several device architectures have been reported in the past aiming at achieving this [2].

2.4 a. Single layer solar cells

This simple architecture consists of a single organic layer sandwiched between the anode and cathode electrodes as shown in Figure 2.2. An electric field results from the difference in the work function of the contacts as in Schottky diodes. Upon incident light, absorbed photons generate excitons which diffuse towards the electrodes where they may dissociate to yield charge pairs. Only those excitons that are created within the layers of the organic material that lies within the exciton diffusion length of a contact can contribute to the photocurrent. In this structure some photons have the chance of being reflected by the back contact and thus have another chance to be absorbed in the film.

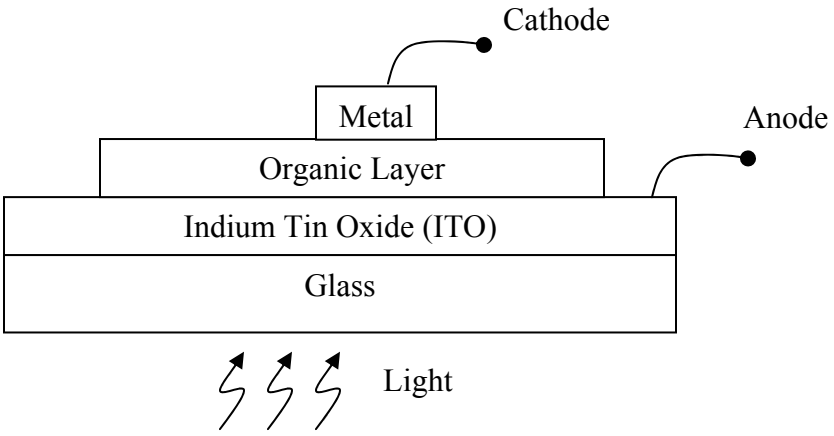

Figure 2.2: Device structure of single layer organic solar cell

2.4 b. Bi-layer solar cells

A bi-layer organic solar cell shown in Figure 2.3 comprises of a donor-acceptor heterojunction. Excitons created by the absorption of photons reach the donor-acceptor interface and are broken up by the local electric fields resulting from the difference in the electron affinity and ionization potential of the two materials. Typically these local electric fields are strong and may break up photogenerated excitons provided that the differences in potential energy are larger than the exciton binding energy. In a bi-layer device the organic donor-acceptor interface separates excitons much more efficiently than the organic-metal interfaces in a single layer device [14].

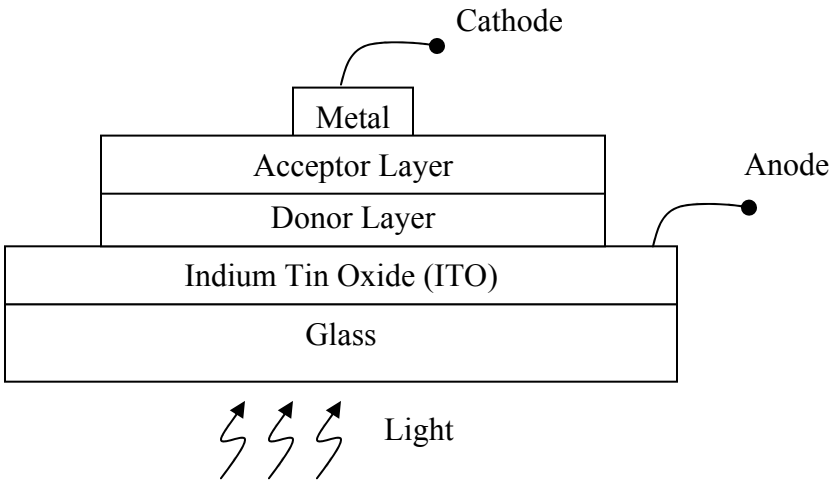

Figure 2.3: Device structure of bi-layer organic solar cell

2.4 c. Multi-layer solar cells

Multi-layer organic solar cells, in addition to the donor and acceptor layers comprise of an additional layer of either an organic or inorganic material. This is illustrated in Figure 2.4. This additional layer was either a thin layer of lithium fluoride (LiF) or bathocuproine (BCP). BCP has been found to transport electrons to the cathode from the adjoining acceptor layer while effectively blocking excitons in the lower energy gap acceptor layer from recombining at the cathode [15]. The use of an interfacial LiF layer has been shown to lower the effective work function of the aluminum cathode and also leads to subsequent doping of the organic layer [16]. Also, variations on this basic structure, including adding an additional layer of the inorganic semiconductor cadmium sulphide (CdS), were investigated with a view toward understanding the behavior of an organic-inorganic junction.

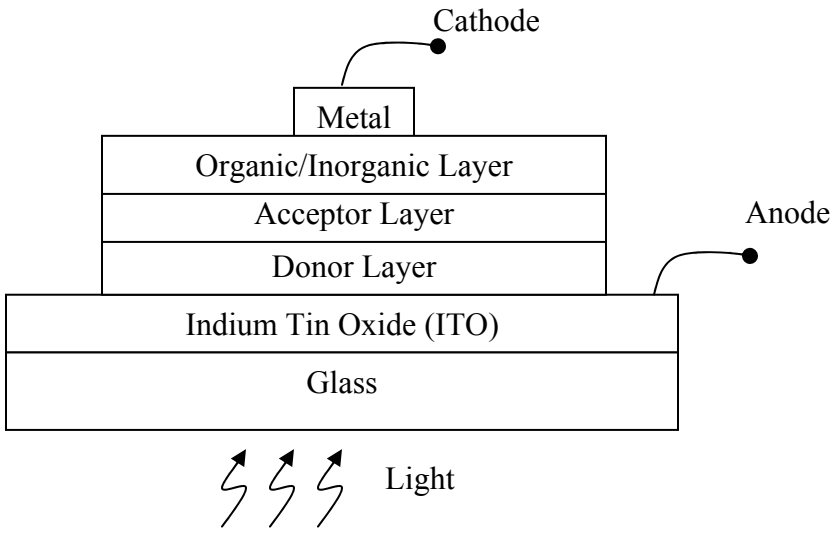

Figure 2.4: Device structure of multi-layer organic solar cell

Chapter 3. Experimental

3.1. Device fabrication

3.1 a. Device structure

The basic device structure of the organic semiconductor based solar cell fabricated in this work is illustrated in Figure 3.1. The solar cell is composed mainly of six important layers; a glass substrate, a transparent conductor layer of ITO (indium tin oxide) as the bottom contact, a conductive polymer layer (Pedot:PSS), a p-type organic copper phthalocyanine (CuPc) layer, an n-type organic 3,4,9,10-perylenetetracarboxylic bisbenzimidazole (PTCBI) layer, and a metal electrode to serve as the top contact. The p-type CuPc layer acts as the absorber layer in this structure. Additionally a thin layer of LiF was also deposited between PTCBI and the metal electrode. And in certain cases an additional exciton blocking layer such as BCP was sandwiched between PTCBI and the metal electrode. Light is shone from the bottom glass side as indicated in Figure 3.1. Devices that included a polymer layer were fabricated by inserting the polymer layer between the ITO and CuPc layer.

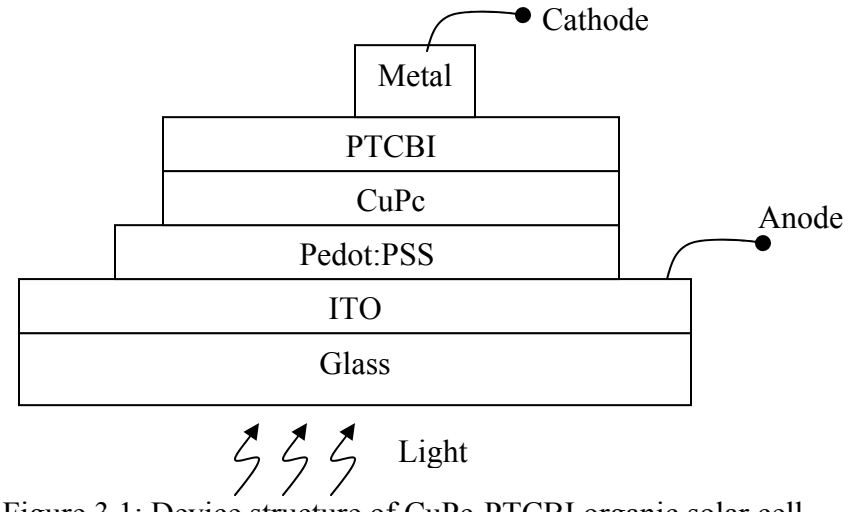

Figure 3.1: Device structure of CuPc-PTCBI organic solar cell

3.1 b. Substrate preparation

ITO coated glass substrates were commercially obtained from Delta Technologies. The sheet resistance of ITO was between 4 to 6 ohms and its thickness was approximately 150 nm. The ITO coated glass was received in sheets of 10 cm x 10 cm in area from the supplier. They were then cut into 1 inch x 2 inch pieces for use in our work. Each experiment was performed using these 1 inch x 2 inch substrates. The cleaning of these ITO substrates involved the following processes. Each substrate was first rubbed with cotton dipped in acetone to remove any visible contaminations followed by ultra sound assisted sonication in acetone for 15 minutes. The substrate was then rinsed in a stream of deionised water and then immediately subjected to sonication in methanol for another 15 minutes. Finally, the substrate was sonicated in deionised water and then dried using a stream of nitrogen. As the effectiveness of cleaning of the substrates has a strong effect on the adhesion properties of the deposited films care was taken during the entire process by handling the substrate with a tweezer, since even handling of the substrates with rubber gloves does not ensure against contamination of the substrates [17]. Also each substrate was cleaned by the above procedure prior to the start of each experiment in order to prevent the oxidation on the surface of ITO over time.

3.1 c. Spin coating

Cleaned ITO substrates were immediately spin coated with a layer of Pedot:PSS using a Chemat model two stage spin coater. The two stage spin coater enables dispensing of the polymer solution onto the substrate at low speeds and homogenizing the coating at high speeds. Pedot:PSS used in the experiments were commercially obtained from two different suppliers: Aldrich Chemicals and Bayer Corporation. The difference in the properties of the Pedot:PSS solution obtained from the two suppliers was in their resistivities which are approximately 0.02 ohm-cm and 1 ohm-cm, obtained from Aldrich and Bayer respectively. Pedot:PSS was spin coated at 4000 rpm and for a time of approximately 40 seconds. The layer was then annealed in a vacuum oven at 100° C for 15 minutes [15]. The reason for annealing is to remove any excess water molecules present in the Pedot:PSS film and also to increase its adhesion to the underlying ITO substrate.

3.1 d. Thermal deposition

Thermal evaporation process was utilized to deposit the organic films on top of the ITO glass substrate. The general principle of this technique is heating the source material (evaporant) in vacuum and thereby causing it to evaporate. The evaporated vapors condense and deposit upon contact with the substrate which is maintained at room temperature, i.e. essentially at a temperature below the boiling point of the evaporant [17]. The thermal evaporation system consisted of an 18 inch diameter vacuum chamber. It consisted of a turbo and rotary pump capable of providing vacuum levels of 10^{-7} torr. This system was used for the thermal evaporation of the organic materials CuPc, PTCBI, LiF, and BCP and also for the evaporation of metals such as gold, silver, copper and aluminum. Care was taken in cleaning

the system after the completion of the evaporation of each material so as to eliminate contamination problems. The evaporator system had two sources, selected by a source selector switch, which enabled the sequential deposition of any two materials without breaking the vacuum. In our experiments, after the ITO substrates were spin coated and annealed they were loaded immediately into the vacuum chamber. CuPc and PTCBI were loaded in different tungsten boats and were placed in each of the sources inside the evaporation chamber. Deposition of the materials was started only when a base pressure of at least 10^{-6} torr was attained. CuPc was first deposited on the Pedot:PSS coated ITO substrate and to the desired thickness. The rate of deposition and the thickness of the deposited film were measured using a gold plated quartz crystal and monitored using an INFICON crystal monitor. After the completion of CuPc deposition without breaking the vacuum deposition of PTCBI was started and performed till the desired layer thickness was attained. Finally the chamber was let to cool for a few minutes and then vented. The substrates were then taken from the chamber and covered with a shadow mask of area 0.07 cm^2 for depositing the metal cathode in order to define the active area of the device. The chamber was cleaned prior to loading the source with material needed for the deposition of metal electrodes. Based on the design of the experiments gold, silver, copper and aluminum were mainly used as the electrodes. Gold (99.999%) and aluminum (99+%) were purchased from Kurt J. Lesker in the form of pellets. Silver (99.99%) wire was obtained from Alfa Aesar. Copper powder (99.999%) was obtained from Sigma Aldrich. Each metal was deposited using different tungsten boats. After the deposition of the metal electrodes the vacuum chamber was let to cool for a time of 30 minutes to prevent the oxidation of the metals.

3.1 e. Annealing

To understand the effect of temperature on the performance of the organic solar cells, the CuPc-PTCBI based solar cells were subjected to annealing in a vacuum oven. Typical annealing temperatures ranged between 100º C and 200º C and the total annealing time ranged from 5 minutes to 15 minutes. During annealing, the films are heat treated in the oven under vacuum and also when an inert gas such as nitrogen was allowed to flow through the oven. The maximum pressure attainable in the vacuum oven was in the order of 25 inches of Hg.

3.1 f. Deposition of Contacts

The final step in the fabrication of the organic solar cells was applying small dots of high purity silver paste on top of the exposed ITO surfaces. The silver dots were then allowed to dry under room conditions for approximately 10 minutes. Silver paste purchased from Ted Pella was used. The use of silver paste ensures that a reliable connection is made to the underlying ITO surface and was also observed in our experiments to yield better fill factors. During electrical characterization electrical leads were individually connected to a silver dot and a thermally deposited metal contact of area 0.07 cm^2 to be used as the anode and cathode respectively. Approximately, there were 30 devices on a single ITO substrate.

3.2. Electrical characterization

The organic solar cells were characterized by current-voltage measurements studied under dark and light conditions. Measurements under light were performed at room temperature using an in-house built solar simulator and measurement instruments that were automated with a computer. In this work, electrical characterizations were performed on each of the 30 devices that were fabricated on a single ITO substrate. The results obtained indicate a deviation of ±150 mV and ±1 mA/cm^2 for the V_{oc} and J_{sc} values respectively. The different experiments conducted for the same device structure indicated a high degree of reproducibility and the highest V_{oc} and J_{sc} values obtained are presented in this work.

3.2 a. Solar simulator

Current-voltage measurements under light were performed using a solar simulator that uses a ENX type Eiko Halogen lamp calibrated with a commercial silicon solar cell (V_{oc}~550 mV, J_{sc}~0.3 A). The lamp is housed inside a black bodied rectangular metal case and cooled by a small fan at the base. The test samples are placed at the top of the metal housing separated by a distance of 15 inches from the light source. This distance was determined during the calibration measurements done with the commercial silicon solar cell and the light source to simulate one sun illumination conditions. Pressure contacts were used to make contact with the silver paste (anode) and the metal electrode (cathode) and were connected to the measurement instruments.

3.2 b. Current – voltage measurement system

As represented in Figure 3.2, the current-voltage measurement system consists of a Kepco bipolar power supply used as a dc voltage source. The voltage across the device under test was measured using a Keithley 2000 digital multimeter. The current delivered was measured using a Keithley 2001 digital multimeter. The instruments are connected to a dedicated computer and are controlled by software program through its IEEE-488 General Purpose Interface Bus (GPIB) interface card. The software program was designed specifically for current-voltage measurements using the LabVIEW Virtual Instrument (VI) software. In tracing the I-V curves the user is required to specify the voltage range, time delay between each incremental measurement and the area of the device being measured as inputs to the program. The program is then executed from the specified starting voltage to the ending voltage and the current voltage measurements are recorded. Using the supplied device area, the program automatically calculates the current density corresponding to each current value obtained. The data is recorded as an ASCII file in the path specified by the user and can later be retrieved to plot the J-V curves.

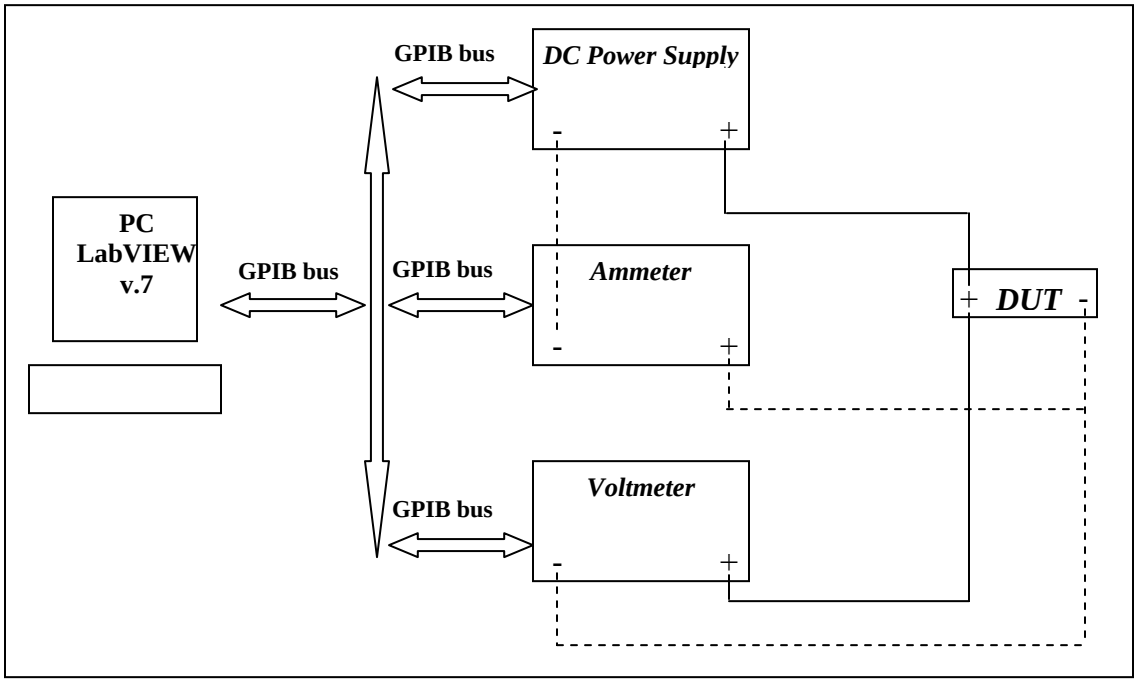

Figure 3.2: Block diagram representation of I-V measurement system

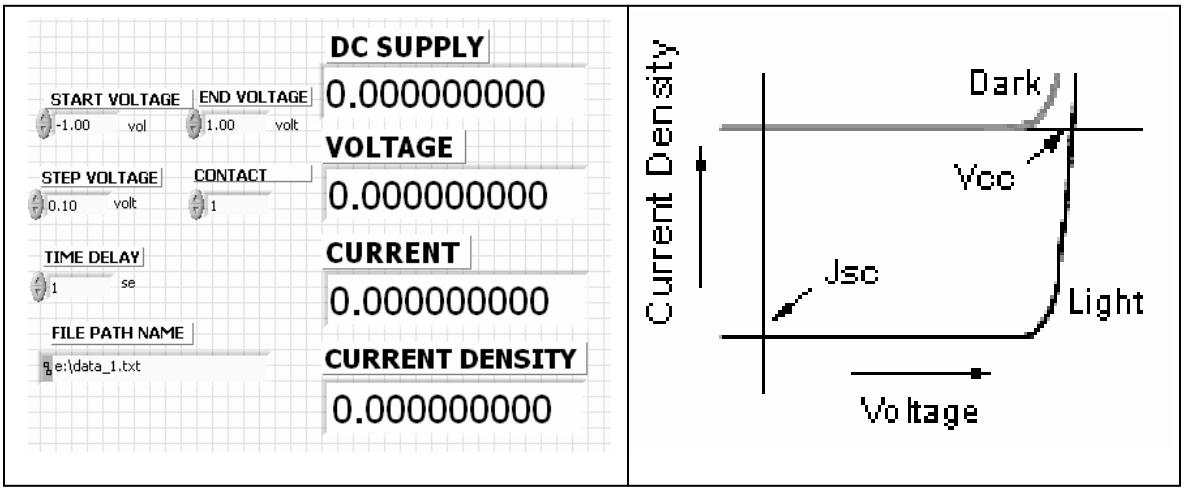

Figure 3.3: Snapshot of the I-V measurement LabVIEW program and ideal J-V curves of a solar cell.

3.3. Material characterization

3.3 a. UV-Vis

Optical absorption studies were carried using an UV-Vis spectrophotometer, which provided detection in the range of 300 nm to 1000 nm. The system is connected to a computer, and the software after interpreting the data from the spectrophotometer presents it to the user in ASCII format. Optical absorption studies were carried out using ITO coated glass or quartz glass as the substrate on which the organic semiconductor was coated and using a similar ITO coated glass or quartz glass as the reference.

3.3 b. SEM analysis

Scanning electron microscopy studies was performed using a Hitachi S-900 FE-SEM. Using the SEM analysis the surface morphology of CuPc, PTCBI and LiF was studied in this work.

Chapter 4. Results

4.1. Single junction organic solar cells:

4.1 a. Pedot:PSS diode

Devices with the structure of ITO-Pedot:PSS-100 nm Aluminum were fabricated and the electrical characteristics of these polymer Schottky diodes were studied. Figure 4.1 shows the current voltage characteristics of the device. It can be seen that the device shows an excessive series resistance due to its low conductivity. Also, it does not display any photovoltaic behavior.

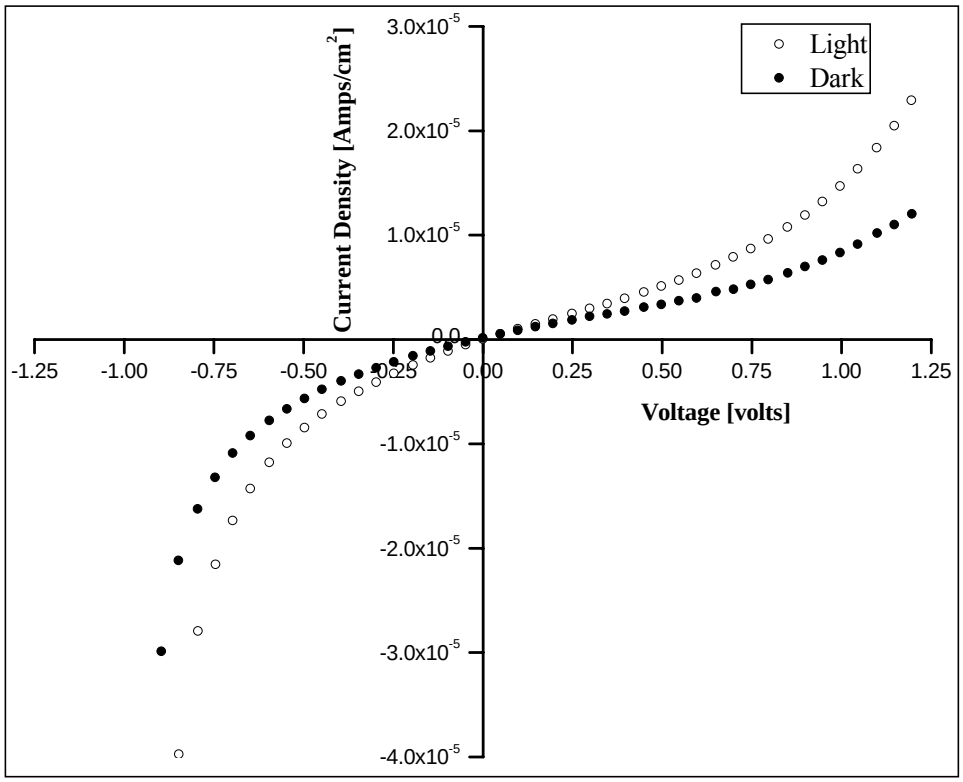

Figure 4.1: J-V curves of ITO-Pedot:PSS-100 nm Al device.

4.1 b.PTCBI diode

In this work devices of the structure ITO-Pedot:PSS-7 nm PTCBI-100 nm Aluminum devices were also fabricated and their electrical characteristics studied. The current voltage characteristics are shown in Figure 4.2. The device structure displayed a photovoltaic effect with a V_{oc} of 150 mV and J_{sc} of 5 $\mu A/cm^2$.

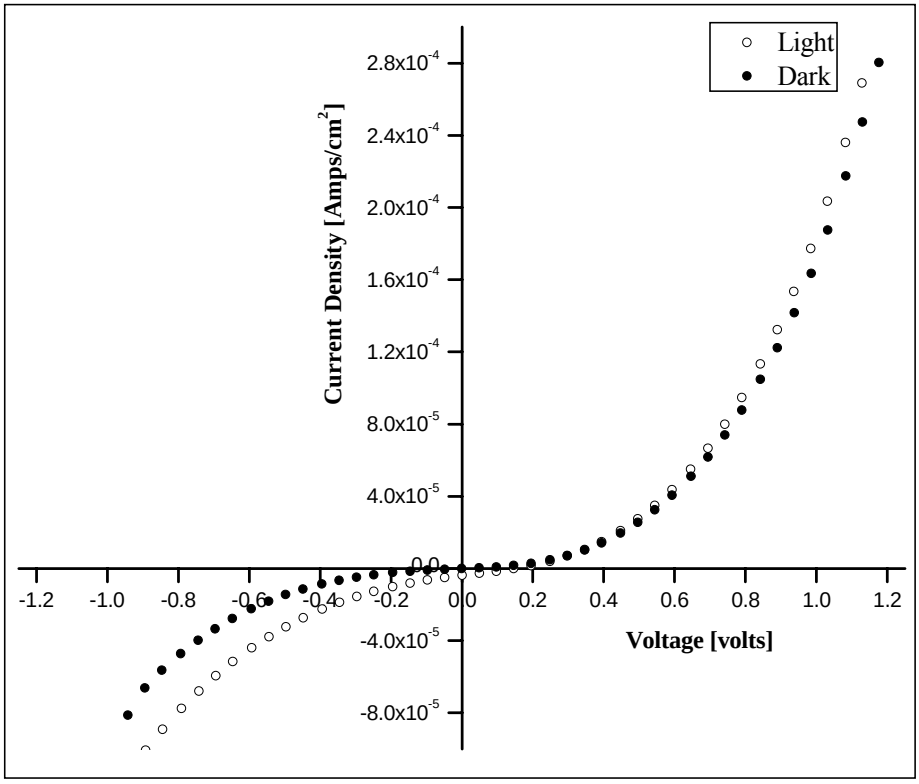

Figure 4.2: J-V curves of ITO-Pedot:PSS-7 nm PTCBI-100 nm Al device.

4.1 c. CuPc diode

ITO-Pedot:PSS-CuPc-Aluminum Schottky diodes were also studied in this work. Two different thicknesses of CuPc layer were investigated. The current voltage characteristics of a 15 nm thick CuPc layer and 60 nm thick CuPc layer are shown in Figure 4.3 and 4.4 respectively. The corresponding V_{oc} and J_{sc} are 150 mV, 0.5 μAmps/cm^2 and 700 mV, 9 μAmps/cm^2 for 15 nm and 60 nm CuPc layers respectively. The increase in the V_{oc} and J_{sc} as the CuPc layer thickness is increased is due to the increased absorption of light in the bulk of the CuPc layer thereby creating more excitons which find their dissociation sites at the CuPc-Aluminum interface. This observation in the increase of the photo voltage with increase thickness in CuPc based schottky diodes is consistent with the results of Kwong et al [18] who have reported an open circuit voltage of 1 V for a 100 nm CuPc layer.

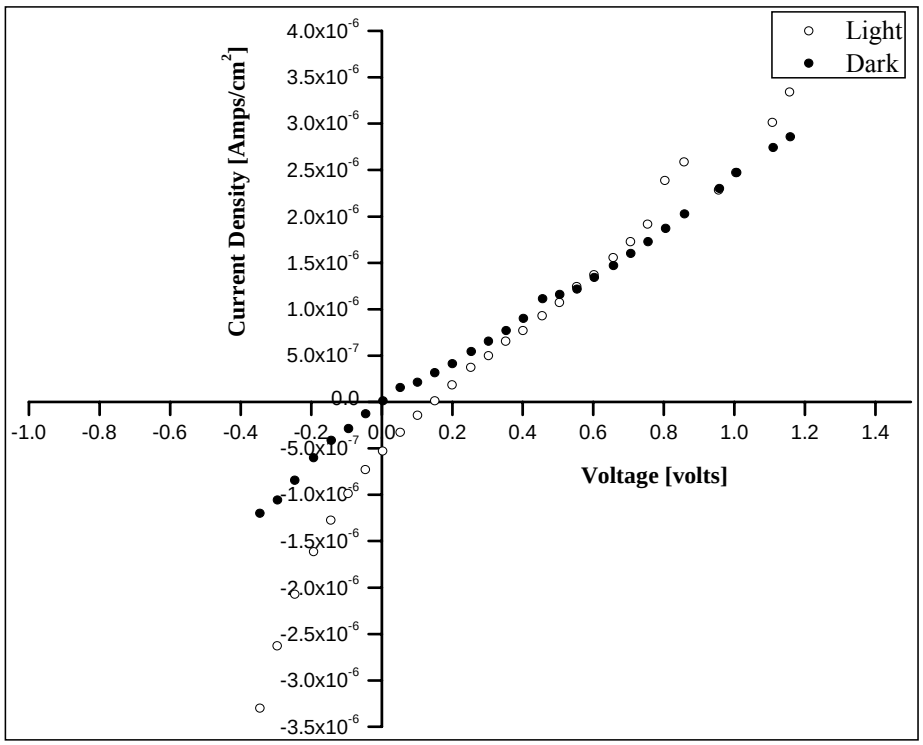

Figure 4.3: J-V curves of ITO-Pedot:PSS-15 nm CuPc-100 nm Al device.

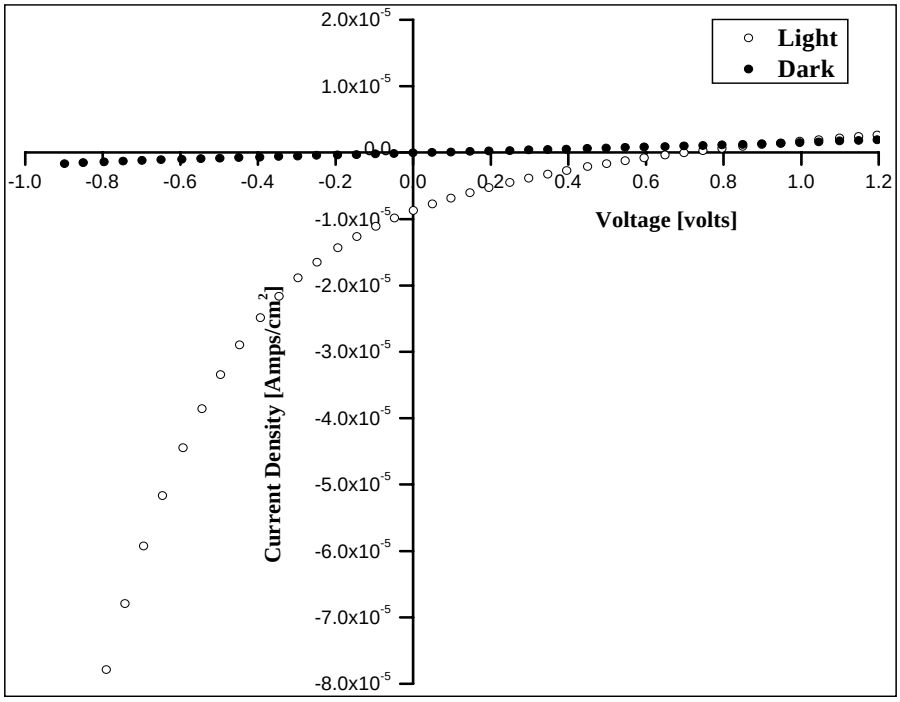

Figure 4.4: J-V curves of ITO-Pedot:PSS-60 nm CuPc-100 nm Al device.

4.1 d. PTCBI doped CuPc diode

In order to determine the effect of adding a PTCBI layer to the ITO-Pedot:PSS-15 nm CuPc device structure a dedicated experiment was carried out. In this experiment a total of twelve devices with a CuPc thickness of 15 nm and an aluminum electrode area of 0.079 cm^2 were fabricated on the same substrate. Half of them included a 15 nm thick PTCBI layer between CuPc and Al while the other half did not. Those with the PTCBI layer exhibited higher voltages and currents. Average V_{oc} and J_{sc} values were 970 mV and 80 mA/cm^2 for the devices with PTCBI, and 150 mV and 0.5 mA/cm^2 for the devices without the PTCBI layer. The J-V curves are shown in Figures 4.5 and 4.6. This experiment proved that the presence of a PTCBI layer seemed necessary for obtaining a high V_{oc} and thereby channeled our research efforts to study the CuPc-PTCBI device structure in detail. Several experiments were carried out based on this device structure and its behavior studied.

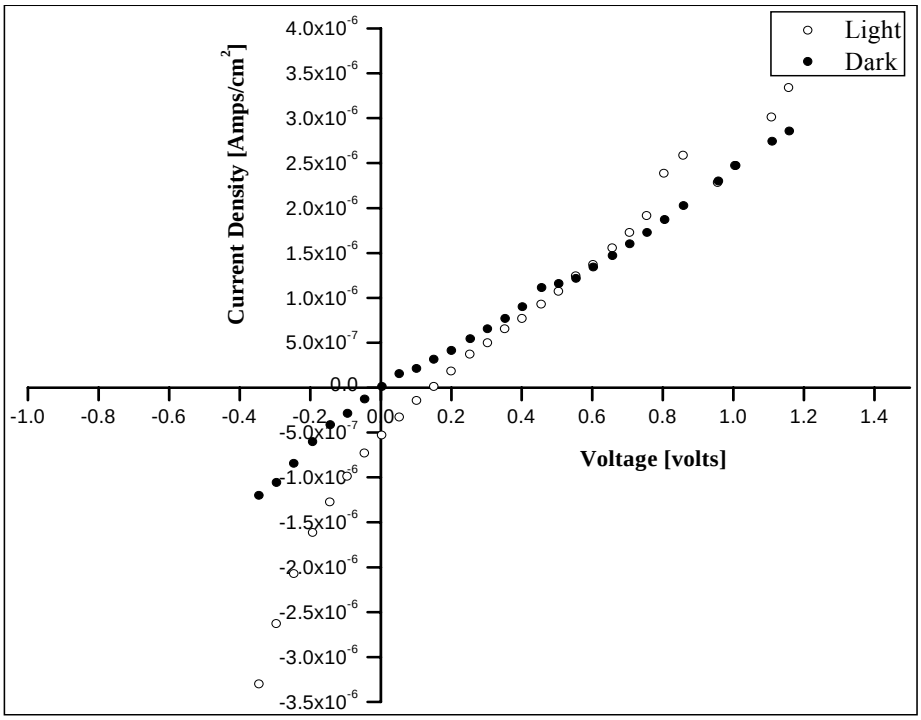

Figure 4.5: J-V curves of ITO-Pedot:PSS-15 nm CuPc-100 nm Al device.

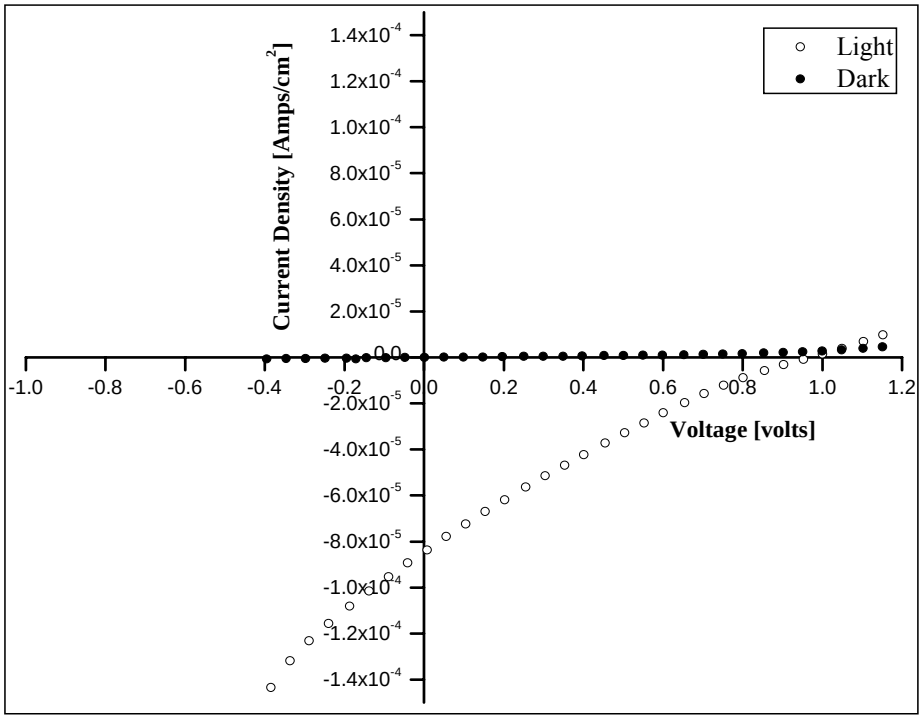

Figure 4.6: J-V curves of ITO-Pedot:PSS-15 nm CuPc-15 nm PTCBI-100 nm Al device.

4.2 Hetero-junction solar cells

4.2 a. CuPc-PTCBI organic-organic junctions

In this work fabrication of organic-organic junctions has been the primary focus. These organic-organic junctions were generally comprised of CuPc-PTCBI as the organic materials. Several devices of this structure with variations in layer thicknesses were fabricated and studied. Figure 4.7 represents the J-V characteristics for the device structure of ITO-Pedot:PSS-15 nm CuPc-7 nm PTCBI-Al.

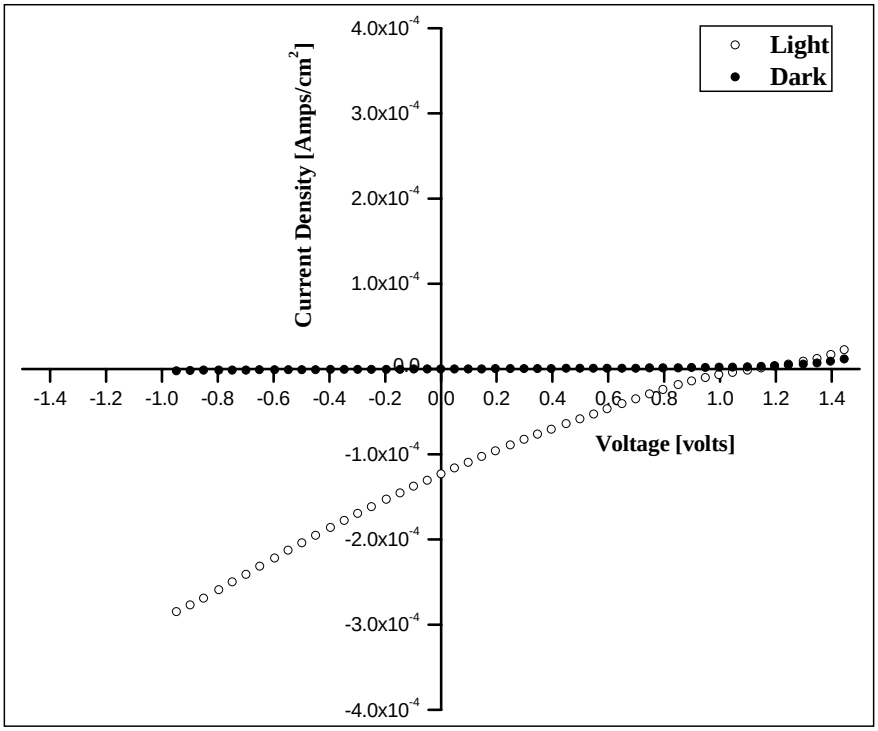

Figure 4.7: J-V curves of ITO-Pedot:PSS-15 nm CuPc-7 nm PTCBI-100 nm Al device

4.2 b. CuPc-CdS organic-inorganic junctions

In an attempt to improve the electrode contact and increase the optical absorption, devices with an organic-inorganic junction were fabricated. CdS was chosen as the inorganic semiconductor in the device structure of ITO-30 nm CuPc-30 nm CdS-Al.

This resulted in a drastic increase in the short circuit current density as shown in Figure 4.8 but at the expense of the open circuit voltage.

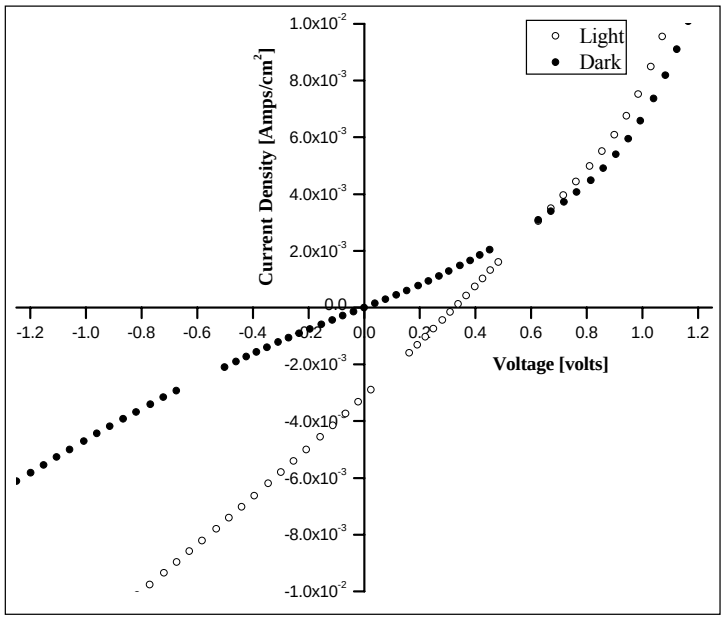

Figure 4.8: J-V curves of ITO-Pedot:PSS-30 nm CuPc-30 nm CdS-100 nm Al device

4.2 c. CuPc-PTCBI-CdS junctions

As previously indicated the addition of a CdS layer contributed to the increase in short circuit current density but with a decrease in the photovoltage. Hence in an attempt to observe high photovoltages, a 10 nm thick CdS layer was added to the CuPc-PTCBI device configuration. First, CdS was introduced between PTCBI and the aluminum electrode and the J-V characteristics were measured. The device with CdS had a V_{oc} of 800 mV and J_{sc} of 0.3 mA/cm^2. Thus a substantial increase in J_{sc} was obtained even though a J_{sc} value of 0.3 mA/cm^2 is still too low. In another variation, 10 nm thick CdS was introduced between the CuPc and PTCBI layers. Here, the device with CdS gave V_{oc} of 950 mV and J_{sc} of 0.03 mA/cm^2. In this case, no advantage in the short circuit current density was obtained. J-V curves for both structures are shown in Figures 4.9-10.

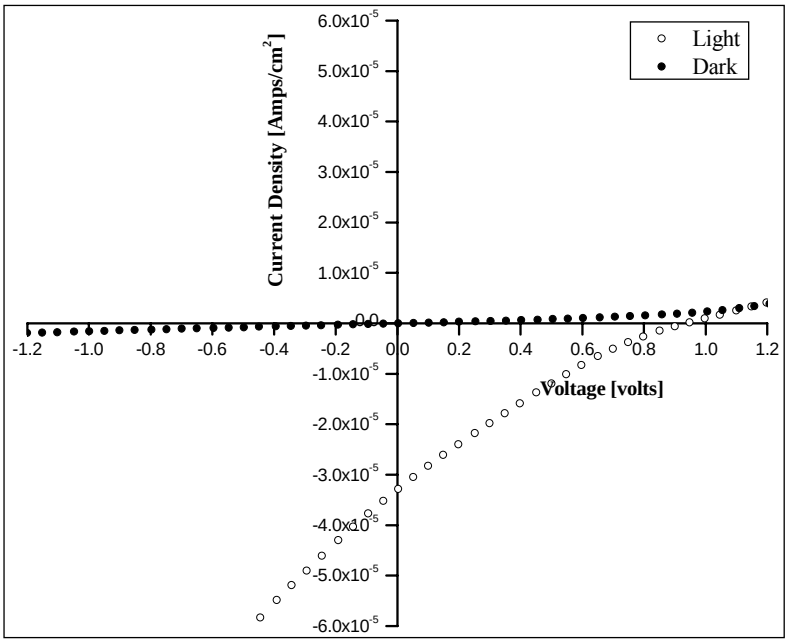

Figure 4.9: J-V curves of ITO-Pedot:PSS-15 nm CuPc-10 nm CdS-15 nm PTCBI-100 nm Al device

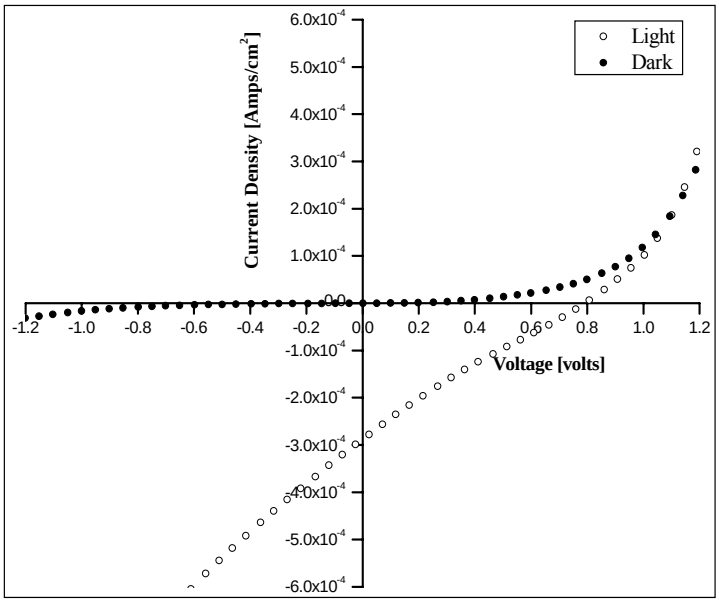

Figure 4.10: J-V curves of ITO-Pedot:PSS-7 nm CuPc-7 nm PTCBI-10 nm CdS -Al device

4.3 Investigation of CuPc-PTCBI junctions

4.3 a. Effect of varying acceptor layer thickness

Optimal thicknesses of donor and acceptor layers in an organic hetero-junction solar cell depend upon their diffusion lengths and absorption coefficients [20]. In order to investigate this design parameter a number of experiments were performed by varying the thickness of the PTCBI acceptor layer while the CuPc donor layer thickness was fixed in the following device structure ITO-15 nm CuPc-X nm PTCBI-100 nm aluminum. The resulting effect on the short circuit current density and the open circuit voltage of the device was studied. A similar experiment was also conducted to study the thickness effect for the above device structure which had a thin layer of LiF deposited between PTCBI and aluminum layers. Figure 4.11 shows the effect of the PTCBI layer thickness on the J_{sc} and V_{oc} while Figure 4.12 shows the corresponding illuminated J-V curves for the devices without the LiF layer. Figure 4.13 shows the effect on the J_{sc} and V_{oc} and Figure 4.14 shows the corresponding illuminated J-V curves for the devices with the LiF layer. In either case the effect of varying the thickness of the PTCBI layer noticeably affected the device's J_{sc} and V_{oc} values. Optimum thickness of the PTCBI layer was hence experimentally found to be between 7 nm and 15 nm for better device performance. This is consistent with the theory that the currents in organic solar cells are limited by the diffusion lengths of the organic layers. For thicknesses lower than the diffusion lengths dissociation at metal interfaces tend to decrease the device currents [2]. For higher PTCBI thickness the R_{series} of the cell is so high that it limits the current instead of adding to it by light-generation and diffusion/recombination.

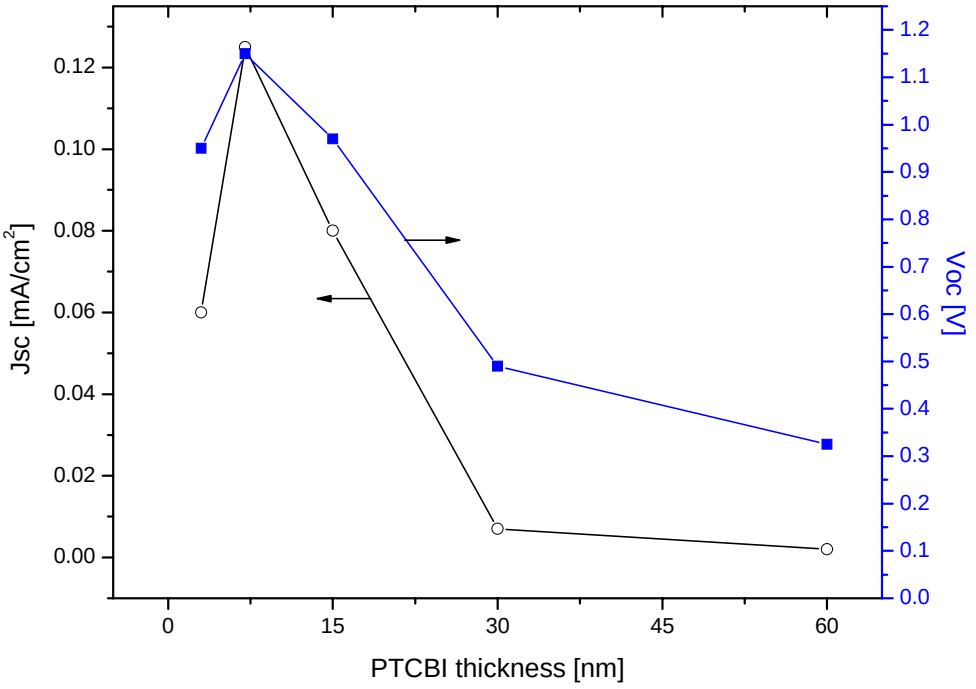

Figure 4.11: Effect of PTCBI layer thickness on J_{sc} (open circles – left axis) and V_{oc} (closed squares – right axis)

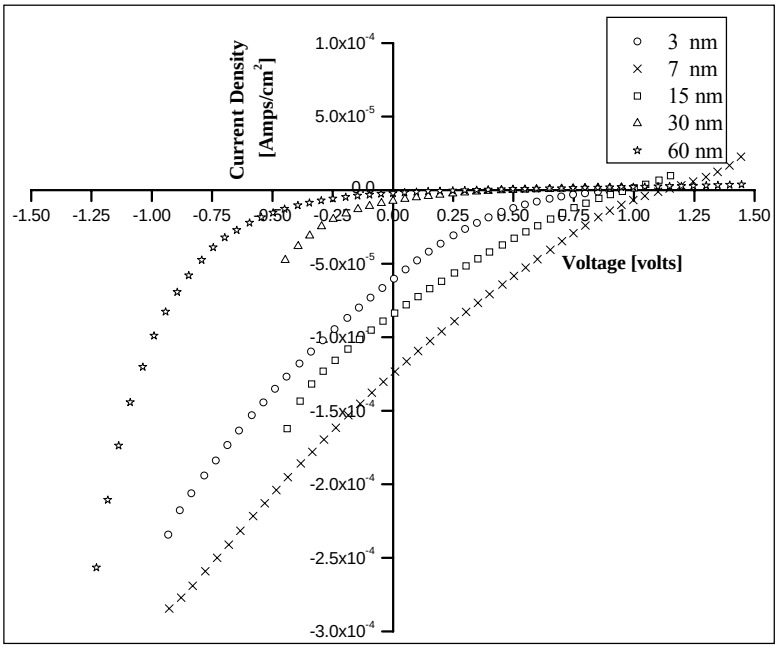

Figure 4.12: Illuminated J-V curves for different PTCBI layer thicknesses of the device structure ITO/Pedot: PSS/15 nm CuPc/X nm PTCBI/Al.

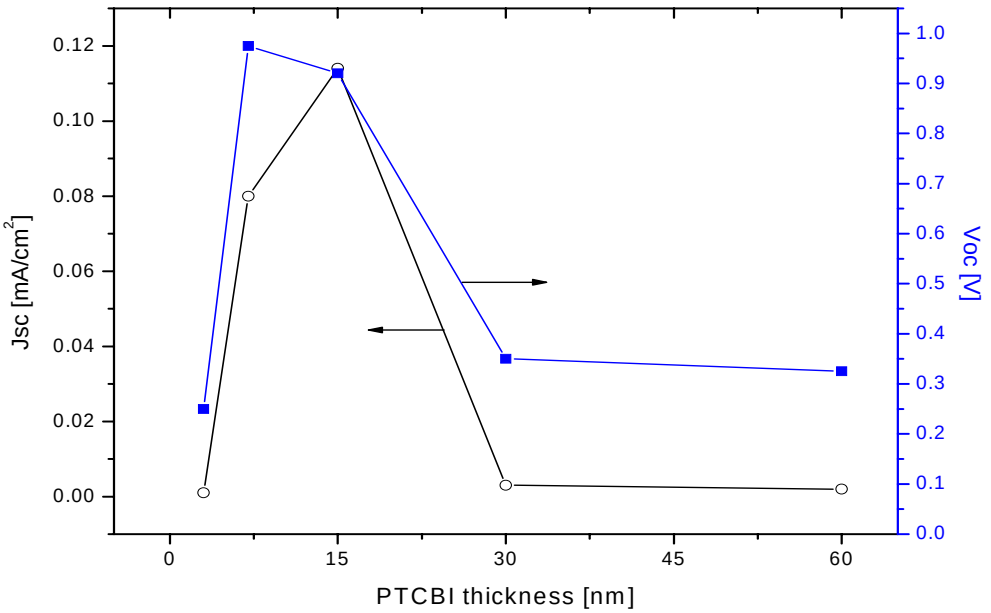

Figure 4.13: Effect of PTCBI layer thickness, with an additional 1 nm LiF layer, on J_{sc} (open circles – left axis) and V_{oc} (closed squares – right axis)

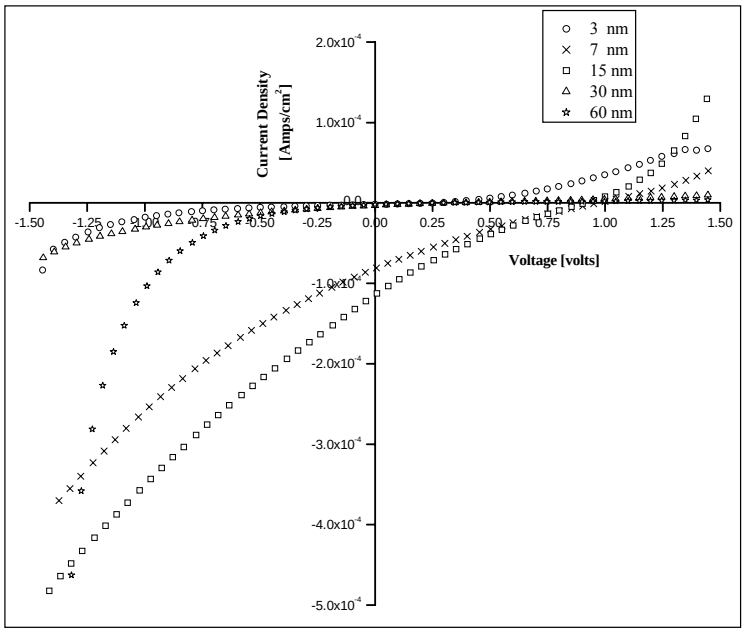

Figure 4.14: Illuminated J-V curves for different PTCBI layer thicknesses of the device structure ITO/Pedot: PSS/15 nm CuPc/ PTCBI/1 nm LiF/Al.

4.3 b. Effect of varying donor layer thickness

The effect of varying the thickness of CuPc layer was also studied through a series of experiments where the thickness of CuPc was varied at 3 nm, 7 nm, 15 nm, 30 nm and 60 nm in the device structure ITO-X nm CuPc-7 nm PTCBI–100 nm Aluminum. The effect of varying the CuPc layer thickness on the short circuit current density and the open circuit voltage is shown in Figure 4.15 and the corresponding illuminated J-V curves are shown in Figure 4.16. Both the short circuit current density and the open circuit voltage are the maximum for a CuPc layer thickness of 15 nm. However at thicknesses of 30 nm the J_{sc} = 0.15 mA/cm^2 is higher than J_{sc} = 0.125 mA/cm^2 which was obtained for a thickness of 15 nm. Though the difference in these values is not significant it could be attributed to the increase in the CuPc layer available for absorption of light. But however the corresponding V_{oc} is seen to be decreased. Also for higher thickness of CuPc i.e. 60 nm both J_{sc} and V_{oc} are greatly reduced. Hence the optimum thickness of CuPc is found to be at 15 nm.

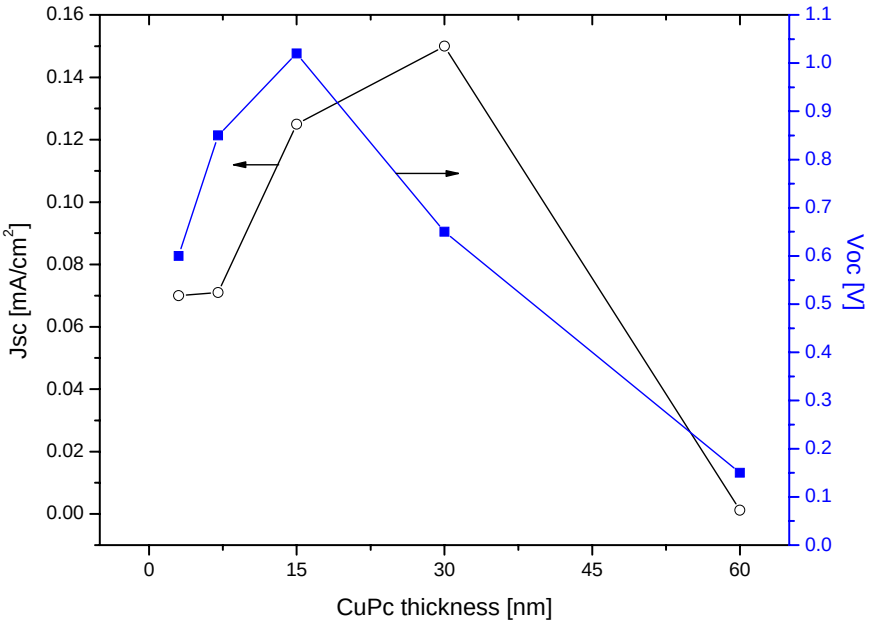

Figure 4.15: Effect of CuPc layer thickness on J_{sc} (open circles – left axis) and V_{oc} (closed squares – right axis) of the devices ITO/Pedot: PSS/CuPc/7 nm PTCBI/Al.

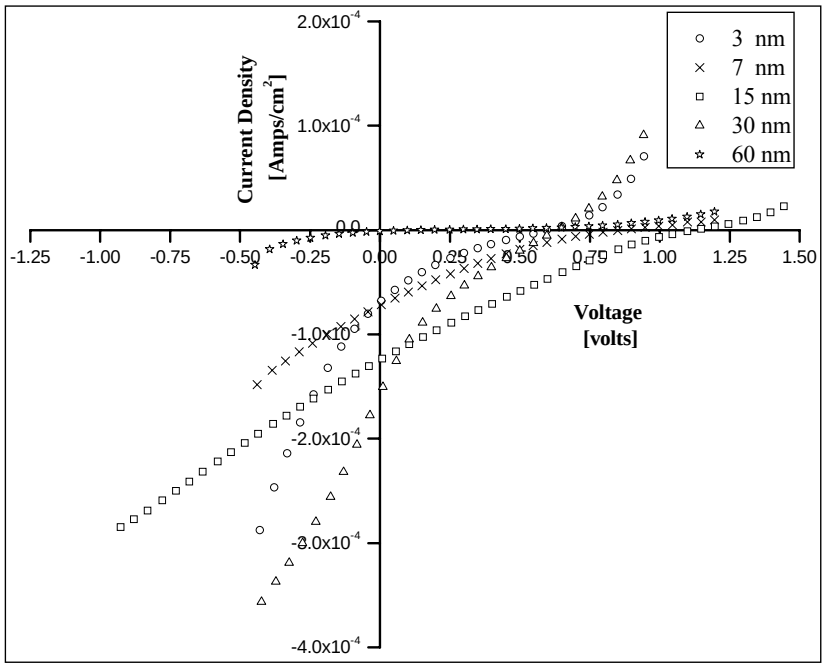

Figure 4.16: Illuminated J-V curves for different CuPc layer thicknesses of the device structure ITO/Pedot: PSS/CuPc/7 nm PTCBI/Al

4.3 c. Effect of Pedot:PSS layer

In order to investigate the role of Pedot:PSS in our device structures we fabricated several devices of the structure ITO-15 nm CuPc-7 nm PTCBI-100 nm aluminum without including the Pedot:PSS layer and also fabricated devices of the same structure but including a Pedot:PSS layer next to ITO. The corresponding J-V curves of devices without the Pedot:PSS layer and that of devices that had a Pedot:PSS layer are shown in Figure 4.17. It can be clearly seen that the V_{oc} is reduced significantly in the case of the device that excluded the Pedot:PSS layer. Also the yield of good devices on the same substrate is much less when compared to the yield obtained from a substrate that had the Pedot:PSS layer. It is understood that Pedot:PSS is mainly used as an interfacial layer to form a better interface between ITO and CuPc by reducing the surface roughness of ITO [19]. It is interesting to note that the short circuit currents in devices with and without a Pedot:PSS layer are similar and only the open circuit voltage is reduced. However the currents at identical bias voltages for a device without a Pedot:PSS layer is much higher than currents for the device with Pedot:PSS layer. It can be attributed to the contribution of Pedot:PSS layer to the increased series resistance of the cell [19].

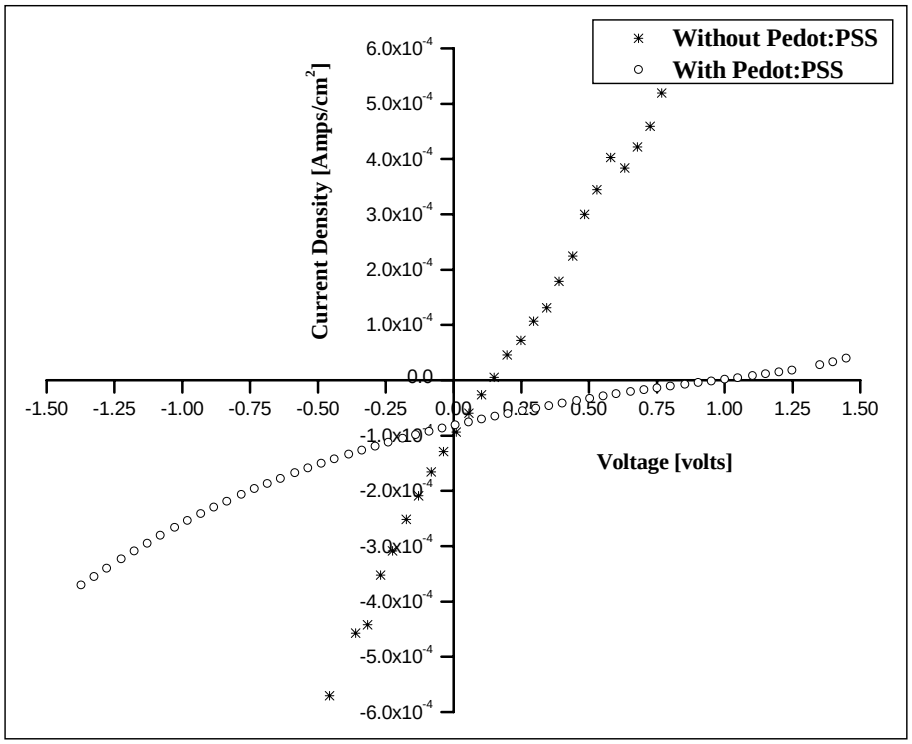

Figure 4.17: Illuminated J-V curves for the device structure ITO/15 nm CuPc/7 nm PTCBI/1 nm LiF/Al with and without an additional layer of Pedot:PSS

Another experiment was conducted to observe the difference in the J-V curves obtained from devices with Pedot:PSS obtained from two different commercial suppliers namely Aldrich and Bayer. However the two Pedot:PSS differ in their electrical conductivities by a factor of 10 but no significant difference was observed in the shape of the J-V curves or in the J_{sc}, V_{oc} values. The illuminated J-V curves are shown in Figure 4.18.

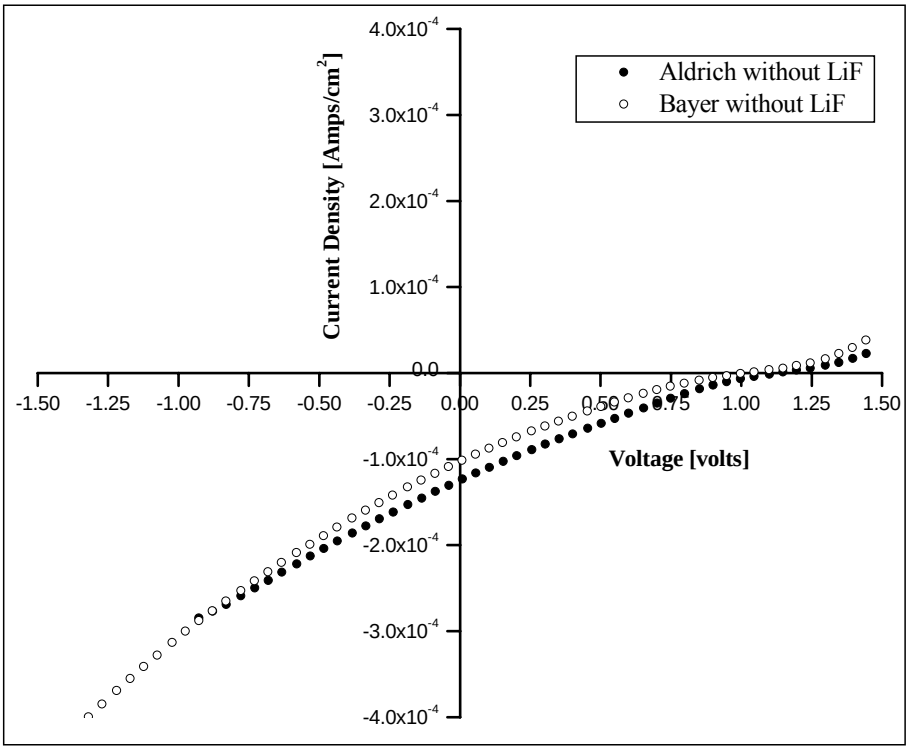

Figure 4.18: Illuminated J-V curves for 15 nm CuPc / 7 nm PTCBI devices using Pedot:PSS purchased from Aldrich and Bayer.

4.3 d. Effect of metal electrodes

The choice of electrode material is critical to the cell performance. Over the last years' research in the area of CuPc-PTCBI solar cells have been focused in using silver as the metal electrode [20]. In this work different metal electrodes were studied and their influence on the device behavior was investigated. Experiments involving the device structure ITO-15 nm CuPc-7 nm PTCBI-metal electrode using aluminum, silver, copper and gold as the metal electrodes were designed. The work functions [21, 22] of these metals are indicated in Table 4.1 along with their densities. All metals were deposited through a shadow mask of 0.07 cm^2 area by vacuum thermal evaporation. It is observed in our experiments that the four different metals due to their difference in their densities required different rates of deposition, with aluminum being the most easiest to evaporate and copper being the most difficult. However with silver and gold, due to their high densities even when deposited at lower rates, the devices mostly resulted in shorts. From our results we understand that since silver and gold are denser metals, during deposition they seem to damage and penetrate the underlying ultra thin (22 nm) organic layers.

Metal	Work Function	Density
Aluminum	4.06 eV	2.70 g/cm^3
Silver	4.26 eV	10.50 g/cm^3
Copper	4.48 eV	8.96 g/cm^3
Gold	5.1 eV	19.32 g/cm^3

Table 4.1: Work function and densities of different metal electrodes used.

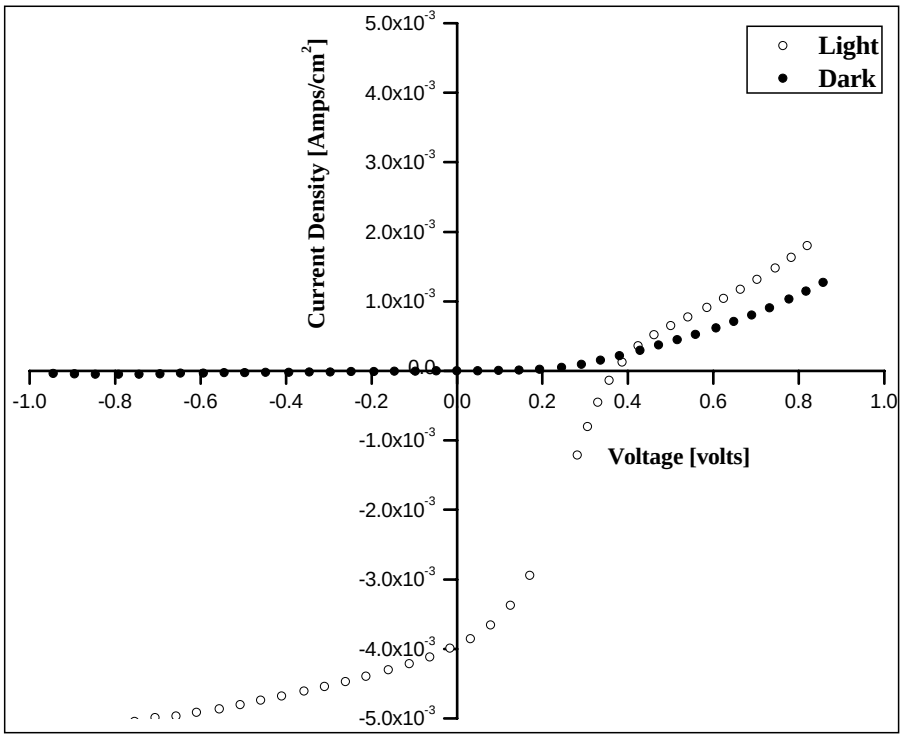

Figure 4.19: J-V curves of 15 nm CuPc/7 nm PTCBI/Ag device

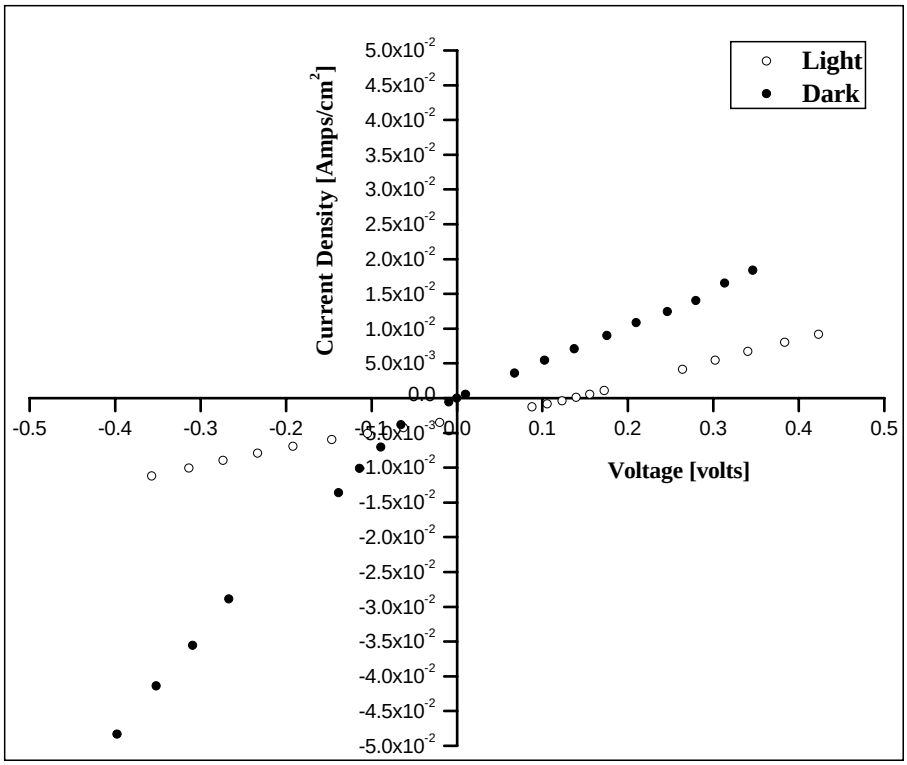

Figure 4.20: J-V curves of 15 nm CuPc/7 nm PTCBI/Au device

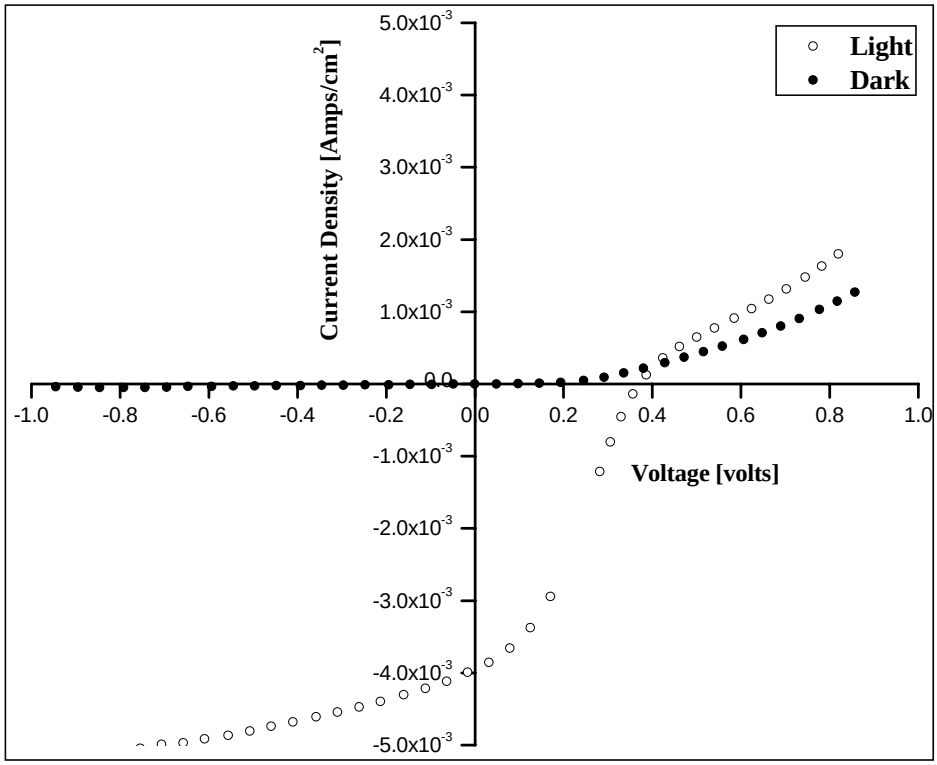

Figure 4.21: J-V curves of 15 nm CuPc/7 nm PTCBI/Cu device

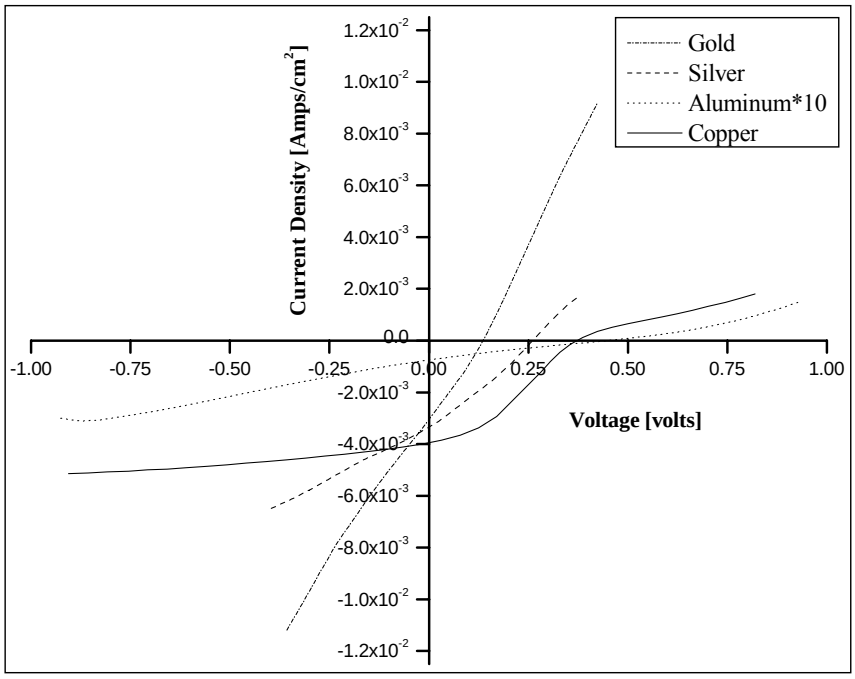

Figure 4.22: J-V curves of CuPc /PTCBI devices with different electrodes.

Figures 4.19-4.21 show the illuminated J-V curves of the device structure ITO-15 nm CuPc-7 nm PTCBI- cathode (silver, gold and copper respectively). As a control experiment all the above metals were deposited on the same substrate with a total of five devices for each electrode respectively. However it can be seen in Figure 4.22, containing all the curves plotted together, that except with aluminum electrode the use of other metals resulted in higher J_{sc}. However in this particular experiment the V_{oc} of the device with aluminum electrodes are around 450 mV as opposed to the expected 1 V value. This is because of the oxidation of the aluminum metal over the period of time required to complete the deposition of the other metals that necessitated the break in the chamber vacuum.

4.3 e. Effect of doping

It is seen from our experiments that the CuPc-PTCBI based heterojunction organic solar cells yielded better performance when the thickness of CuPc and PTCBI layers were fixed at 15 nm and 7 nm respectively. Hence without changing this device design parameter we conducted several experiments on this structure by doping with organic materials such as C_{60}, LiF, BCP and also with inorganic materials such as CdS. The structure was also examined by use of different metal electrodes as mentioned earlier and also with an interlayer such as chromium and alumina underlying the metal electrodes. All experiments were designed using the base structure of ITO-Pedot:PSS-15 nm CuPc-7 nm PTCBI. The corresponding J-V curves are shown in Figures 4.23-29.

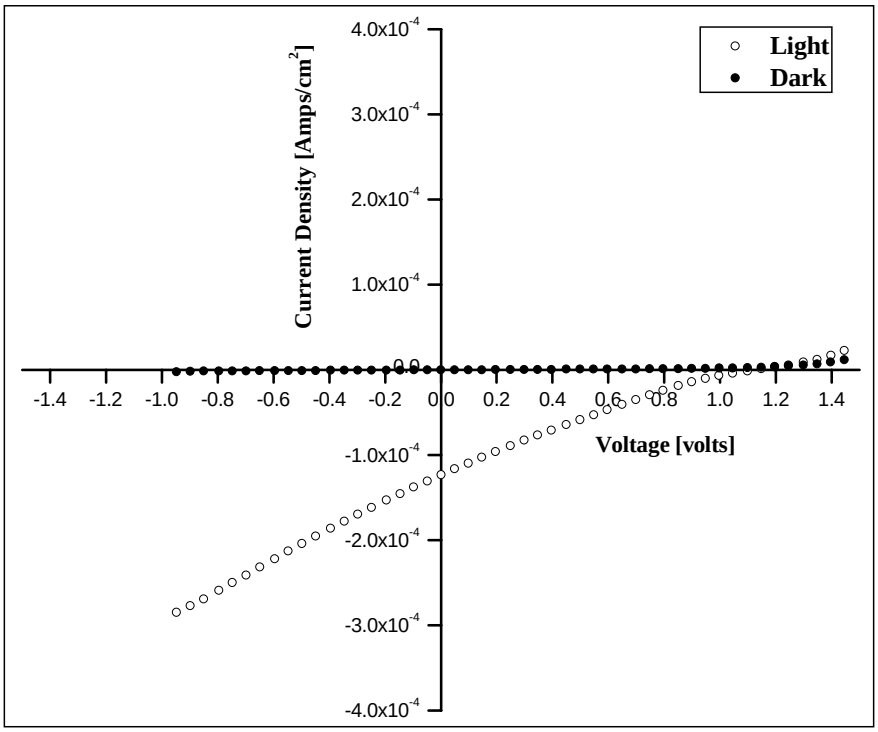

Figure 4.23: J-V curves of 15 nm CuPc/7 nm PTCBI/Al device

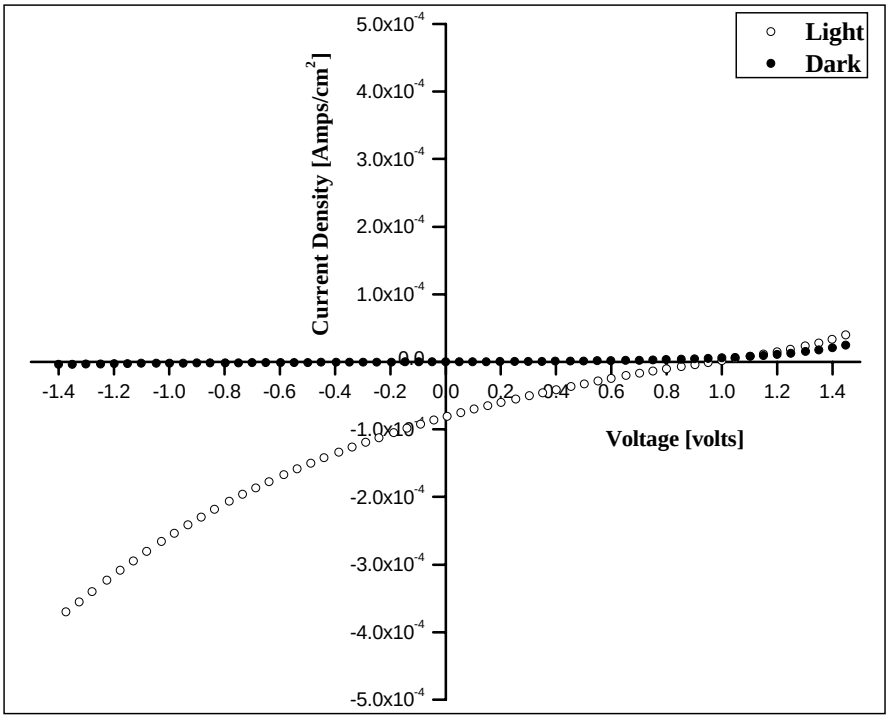

Figure 4.24: J-V curves of 15 nm CuPc/7 nm PTCBI/LiF-Al device

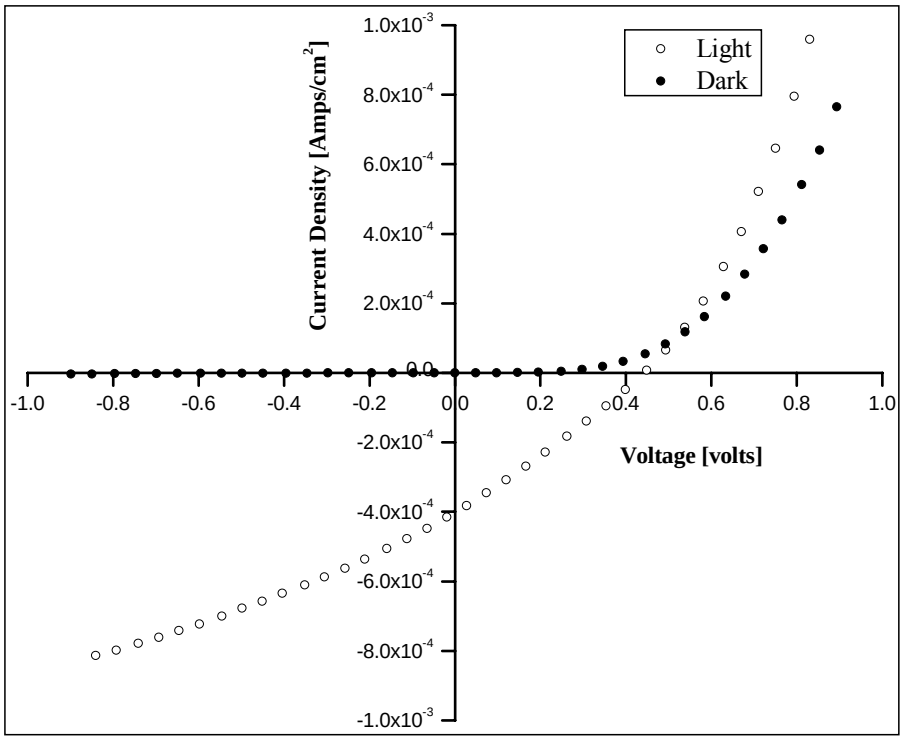

Figure 4.25: J-V curves of 15 nm CuPc/7 nm PTCBI/Cr-Al device

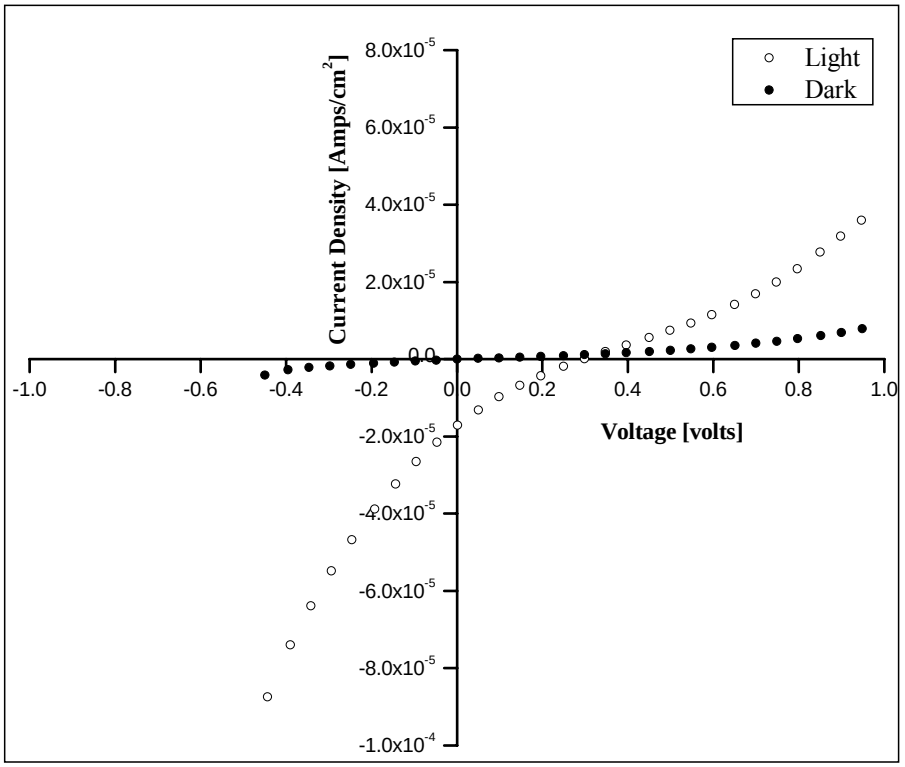

Figure 4.26: J-V curves of 15 nm CuPc/7 nm PTCBI/Al_20_3-Al device

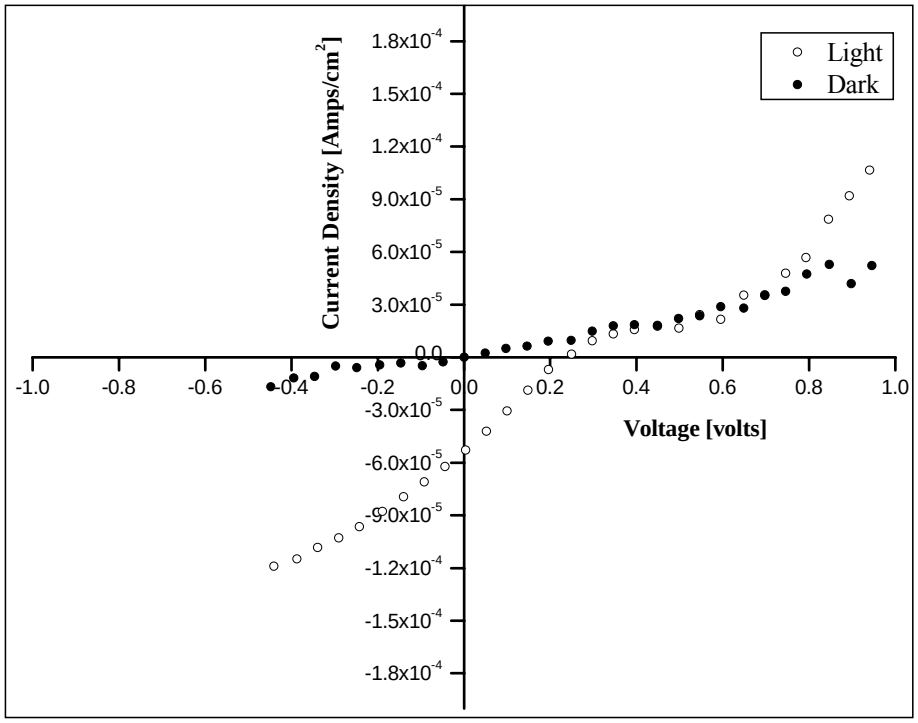

Figure 4.27: J-V curves of 15 nm CuPc/7 nm PTCBI/Al_20_3-Ag device

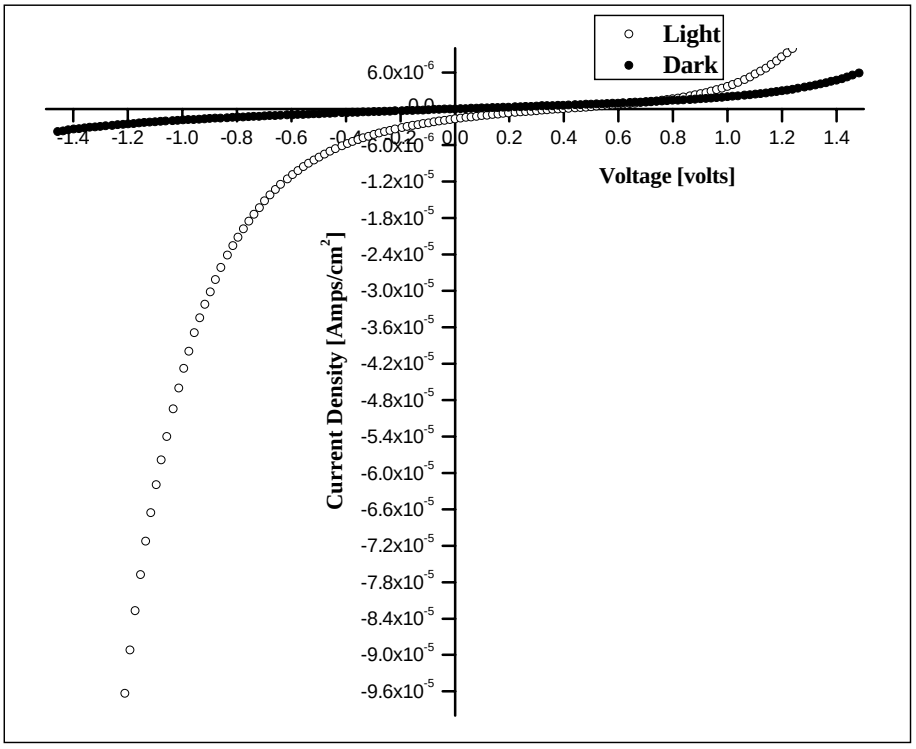

Figure 4.28: J-V curves of 15 nm CuPc/15 nm PTCBI/BCP/Al device

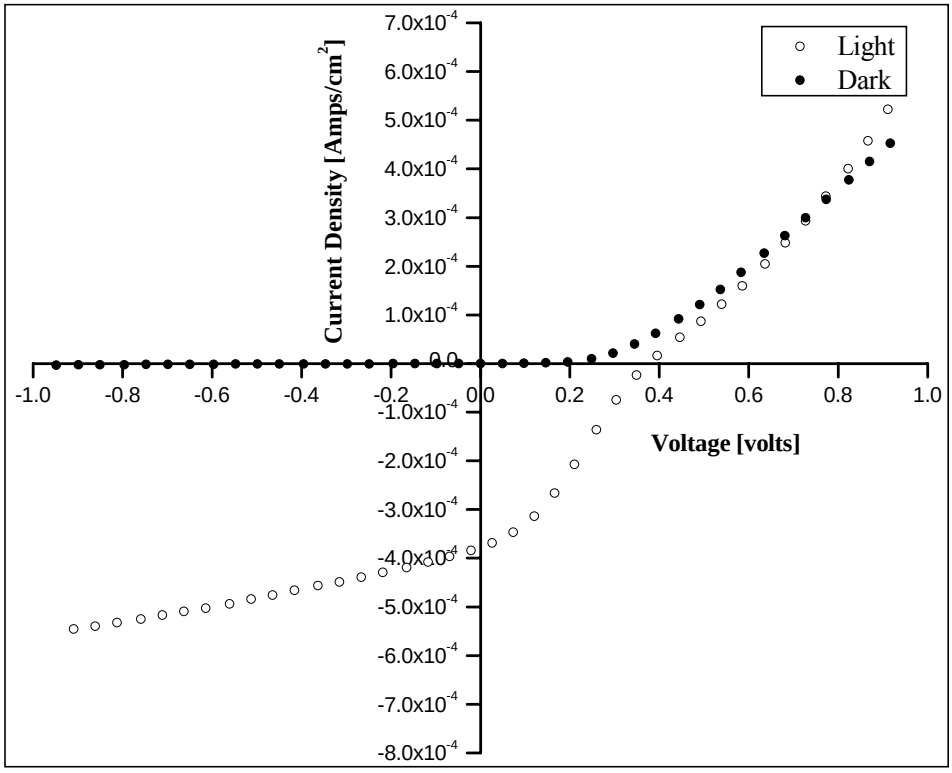

Figure 4.29: J-V curves of 15 nm CuPc/7 nm PTCBI/40 nm C_{60}/LiF-Al device

4.3 f. Effect of annealing

To understand the effect of annealing, a device of the structure ITO-Pedot:PSS-15 nm CuPc-15 nm PTCBI-100 nm aluminum was fabricated and its J-V characteristics was immediately studied without any further treatments. After the I-V measurement was performed, the device was annealed in vacuum at 200° C for 15 minutes and was then measured again. The J-V curves for the same device, before annealing and after annealing, are plotted in the same graph for comparison reasons in Figure 4.30. It is observed that both V_{oc} and J_{sc} decrease significantly due to the effect of annealing. The V_{oc} is reduced by nearly one third and the J_{sc} is 50 times smaller than what was observed before annealing. This deterioration in the device characteristics is because of the degradation effect caused by the crystallization of the organic molecules thereby modifying their electronic properties [23].

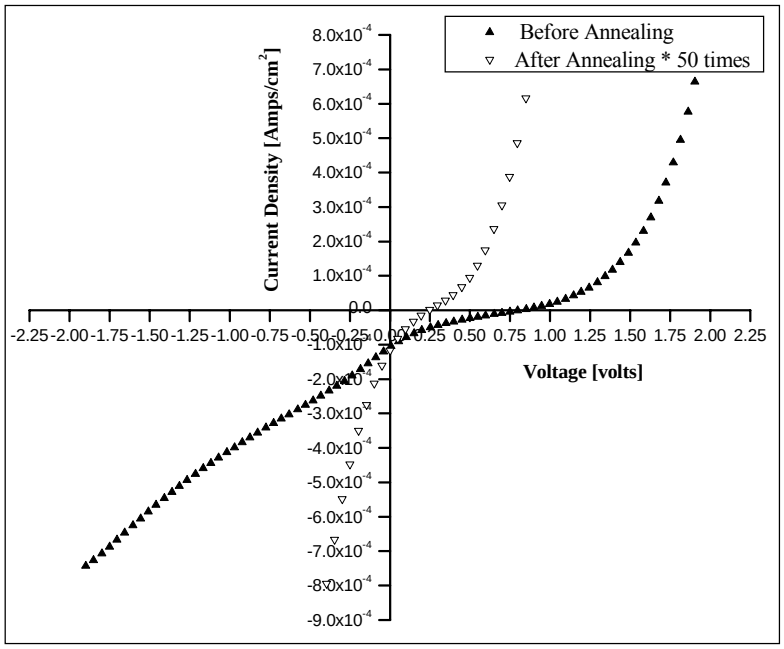

Figure 4.30: J-V curves of CuPc-PTCBI device before and after annealing.

4.3 g. Effect of varying light intensities

The current density versus voltage characteristics of the device ITO-15 nm CuPc-7 nm PTCBI-100 nm aluminum obtained under different illumination intensities varying from 0.6 suns to 1 sun is shown in Figure 4.31. After fabrication, the J-V characteristics of the device was measured at 1 sun illumination intensity and then the illumination intensity was decreased in gradual steps and the corresponding J-V characteristics were measured. After a few measurements under intensities less than 1 sun, the device was measured repeatedly again at 1 sun to make sure that the device had not degraded during the repeated measurements. All measurements shown in Figure 4.31 were obtained from the same device. However, many devices when they were repeatedly measured showed a degrading effect i.e. the J-V curves measured during the second attempt at 1 sun were not identical to the curves measured in the first time. It is understood that the degradation effect is caused by the sensitivity of the organic materials to the environment factors such as temperature, humidity and mainly oxidation due to exposure to oxygen. For reference purposes a commercial solar silicon cell was also subjected to the same sequence of measurements and its J-V curves are also shown in Figure 4.32.

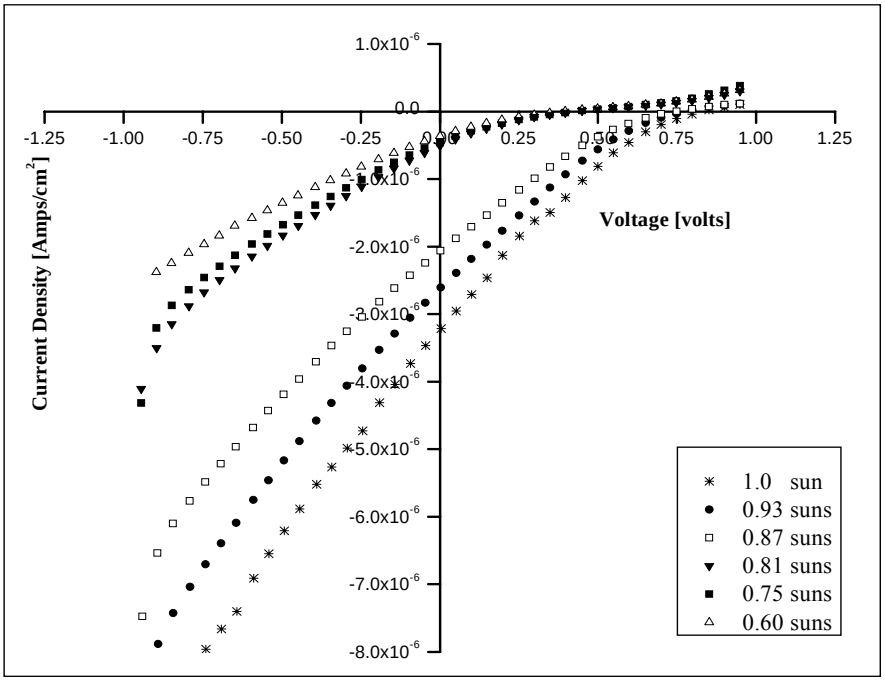

Figure 4.31: J-V curves of CuPc-PTCBI device in varying light intensities

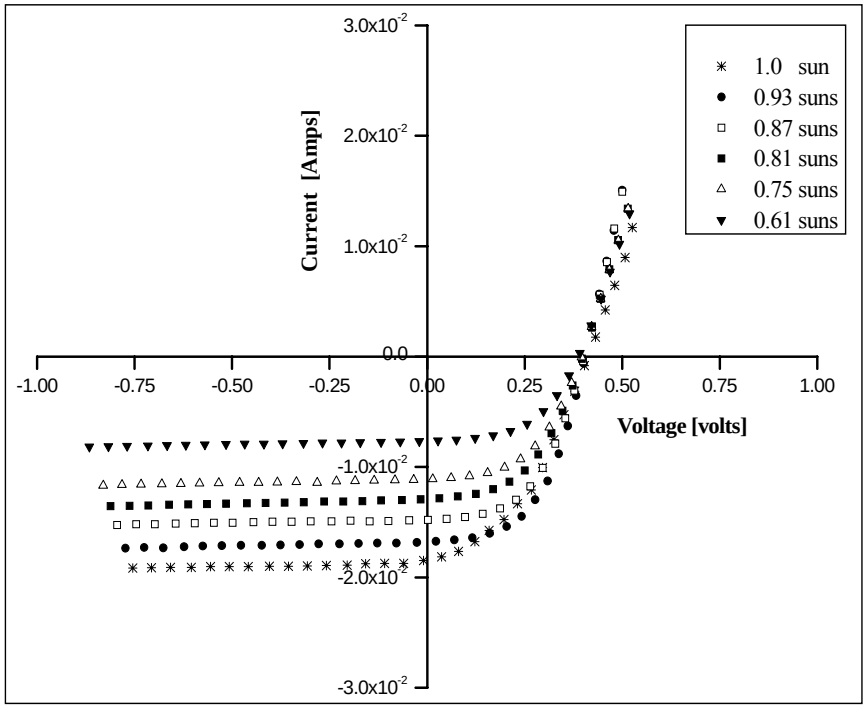

Figure 4.32: J-V curves of silicon solar cell in varying light intensities

4.4 Optical absorption studies

The photo absorbance near the p-n junction, to a major extent determines the properties of a solar cell [24]. Figure 4.33 shows the absorbance spectrum of a 15 nm thick CuPc layer. The CuPc layer shows a peak at around 625 nm and also at 350 nm. However there is an absorbance window between 420 nm and 520 nm where the absorbance in the CuPc layer is minimal. Figure 4.34 shows the absorbance spectrum of 7 nm PTCBI layer. It is observed that the PTCBI layer has a broad absorbance spectrum that spans from 440 nm and 640 nm and peaking at 540 nm. In Figure 4.35 the absorbance spectrum of 15 nm CuPc-7 nm PTCBI film is plotted along with the spectrum of the individual films for comparison. From the absorbance spectrum of 15 nm CuPc-7 nm PTCBI film, it is obvious that the incident light is mainly absorbed in the CuPc layer, as the spectrum is characteristic of the 15 nm CuPc film absorbance spectrum. However incident photons with wavelengths ranging between 420 nm and 520 nm, i.e. the CuPc absorbance window, after passing the CuPc layer will not decay as they get absorbed by the PTCBI layer. It is observed that CuPc layer doped optimally with PTCBI is responsible for the blue shift in the absorption spectra of the CuPc-PTCBI films as seen in Figure 4.35. Forrest et al have reported a similar behavior where a blue shift in the exciton energy in 3,4,9,10-perylene-tetracarboxylic-dianhydride (PTCDA) with decreasing layer thickness is noticed [25].

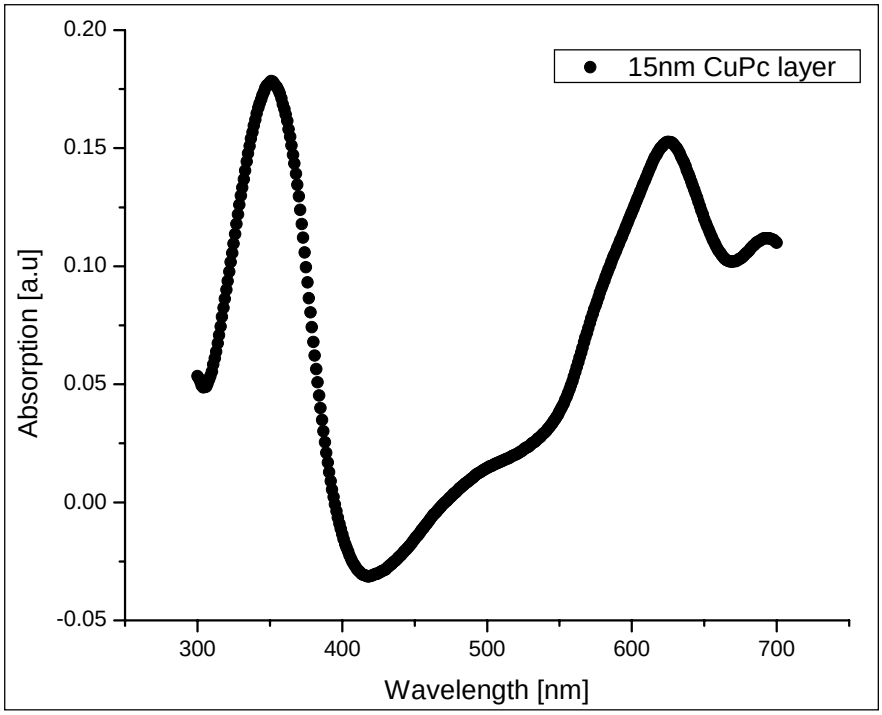

Figure 4.33: Absorbance spectra of 15 nm CuPc layer

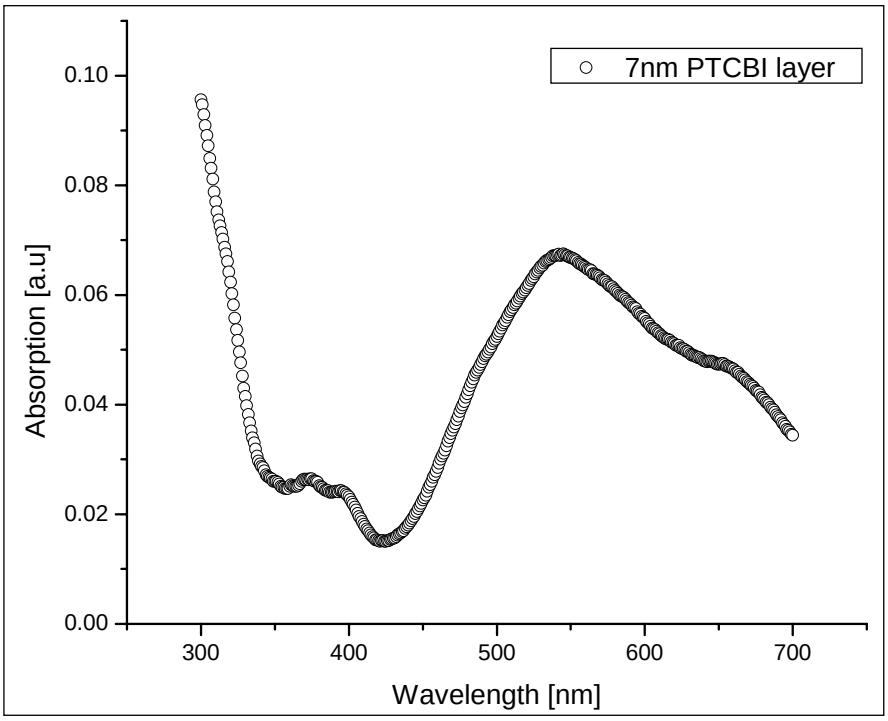

Figure 4.34: Absorbance spectra of 7 nm PTCBI layer

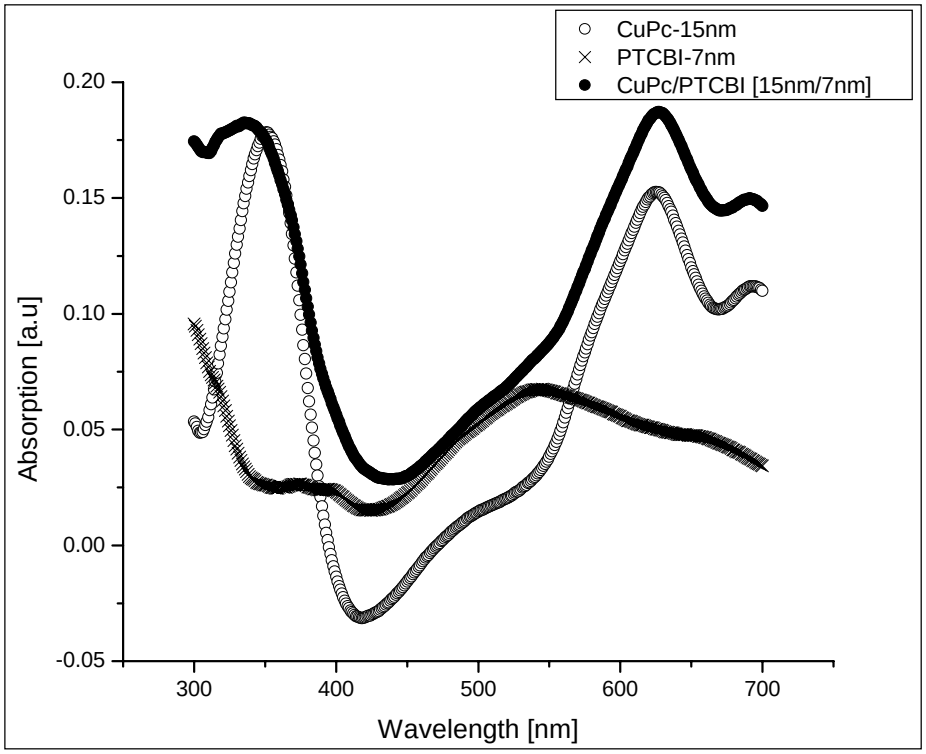

Figure 4.35: Absorbance spectra of CuPc, PTCBI and CuPc-PTCBI layers

4.5 SEM analysis

The surface morphologies of the CuPc and PTCBI organic semiconductors used in the CuPc-PTCBI junction devices were individually studied through electron microscopy analysis. Figure 4.36 shows the morphology of a 15 nm thin CuPc film. The CuPc layer has a typical grain like morphology with average grain sizes of 20 nm. The effect of varying the PTCBI layer thickness was also studied through electron microscopy. Figure 4.37 shows the morphologies of 15 nm CuPc-7 nm PTCBI layer grown on ITO substrates. The 15 nm CuPc layer was first grown on ITO and then 7 nm PTCBI layer was deposited on the CuPc film. The films were grown by thermal deposition at room temperature. Interestingly the SEM analysis reveals the surface of CuPc to show a needle like growth. However the 7 nm PTCBI deposited on top of CuPc is observed as small islands over the needles. It is not clearly understood as to why the needle like growth is observed in the CuPc film grown at room temperature as it is reported that this needle like growth in CuPc films are observed only in CuPc films grown on substrates maintained above room temperature [26].

It should be noted here that the films were not subjected to any heat treatments after being thermally deposited on the substrates. The CuPc grains appear darker under an FE-SEM and PTCBI grains appear as bright spots due to the charging. For PTCBI thicknesses of above 7 nm grown over 15 nm CuPc films the needle like morphology of CuPc films was not observed. But it is also evident that for higher thicknesses of PTCBI films clustering of the PTCBI particles takes place. PTCBI forms aggregates of approximately spherical shape on the surface of CuPc, these aggregates are similar in shape to those observed when only PTCBI is grown on ITO. It is concluded that with increasing PTCBI thickness over an underlying CuPc layer the surface modification suggests a phase separation at the nanoscale

level. CuPc is also known to form a mixed ordered-binary layer with PTCDA even though with sequential deposition of CuPc and PTCDA [27]. Earlier reports by Rudiono et al [28] on perylene doped CuPc films indicate that beyond 9% doping, perylene precipitates as evidenced by electron microscopy studies and decreases the efficiency of the devices. We have also found that with increasing PTCBI layer thickness the device performance characteristics tends to decrease.

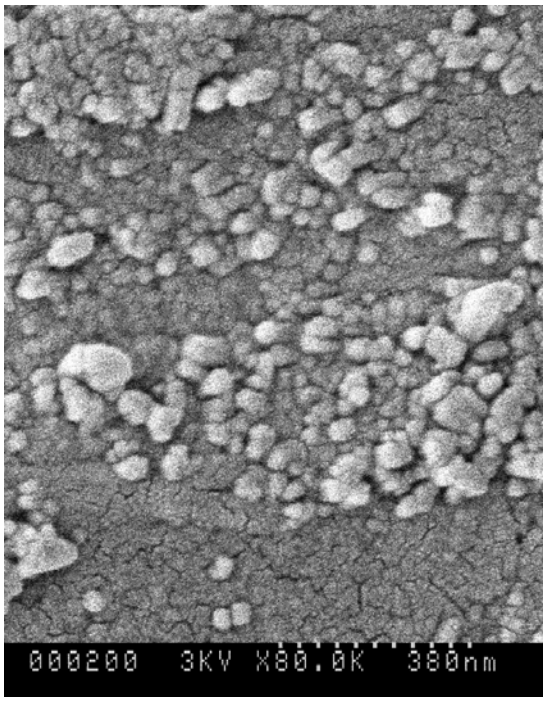

Figure 4.36: SEM analysis image of 15 nm CuPc layer

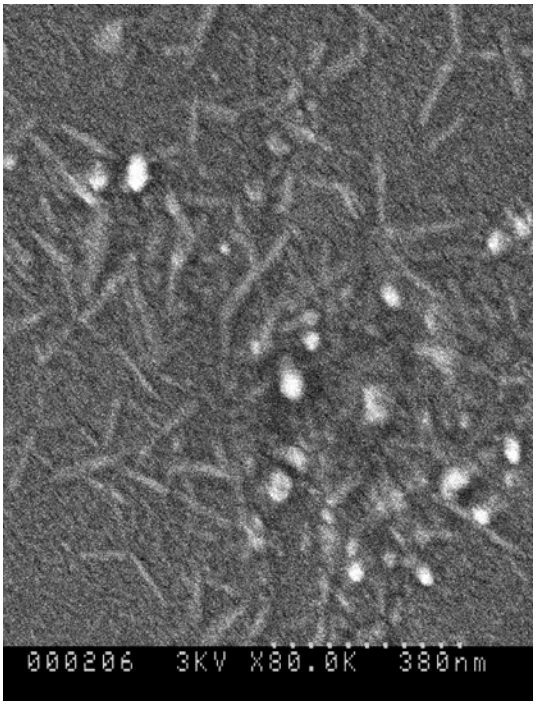

Figure 4.37: SEM analysis image of 7 nm of PTCBI grown over 15 nm of CuPc layer

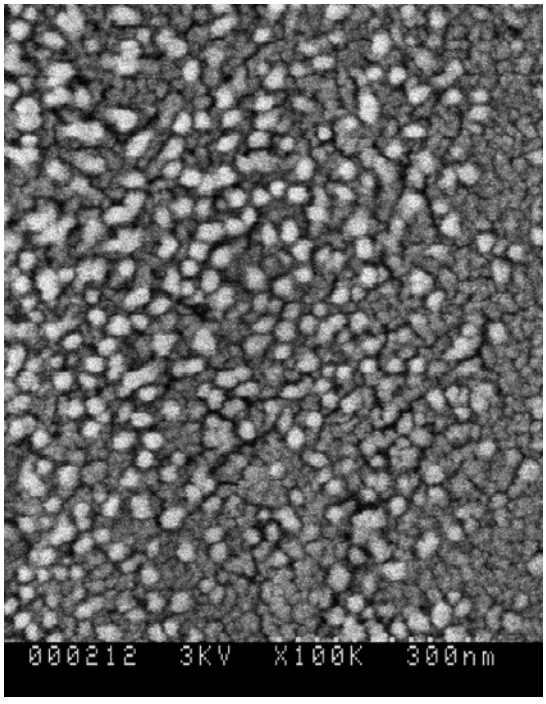

Figure 4.38: SEM analysis image of 30 nm of PTCBI grown over 15 nm of CuPc layer

Figure 4.39 shows the SEM image of a 1 nm LiF film deposited on top of the substrate. As clearly seen from the image the LiF particles are scarcely scattered over the area of the substrate and do no form a continuous film. This supports our results where some devices formed on the same substrate yielded poorer results when compared to other devices on the same substrate. However this difference was not significant to conclude the role of LiF.

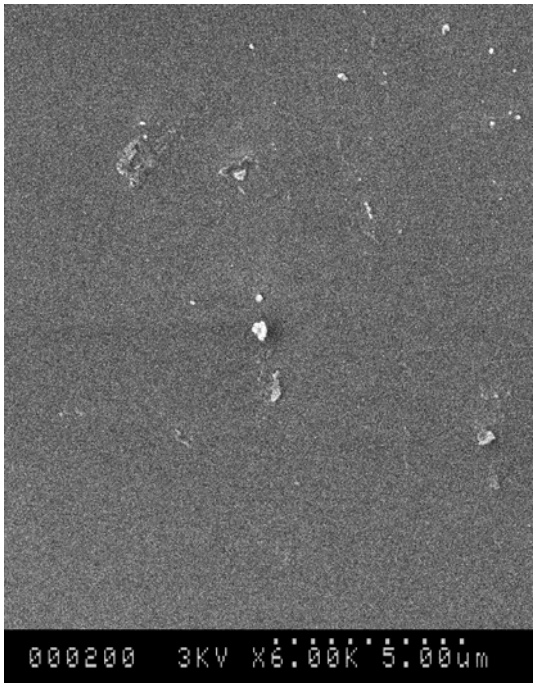

Figure 4.39: SEM analysis image of 1 nm of LiF layer

Chapter 5. Discussion

The results presented in chapter 4 can be understood in terms of a model where the CuPc-PTCBI-Al device with thin (7 nm or less) PTCBI layer is conceived as a Schottky diode between the CuPc layer (modified by thin PTCBI) and aluminum. In other words, the thin PTCBI layer is thought to be entirely incorporated into the CuPc, now described as the ‘‘modified CuPc’’. Energy level diagrams of Schottky diodes consisting of a modified CuPc layer and Al, Ag, Cu and Au electrodes are sketched in Figures 5.1-5.4, respectively. Electron affinity and ionization potential values used in these diagrams were obtained from the literature [2, 29]. In order to arrive at a built-in potential (V_{bi}) value larger than the observed V_{oc} value of 1.15 V, the effective Fermi level of CuPc had to be placed only slightly above (0.05 eV) its highest occupied molecular orbital (HOMO) level. This implies that the modified CuPc must be highly conductive at least at its top surface next to PTCBI. Similarly, the effective Fermi level in PTCBI was placed 0.7 eV below its lowest unoccupied molecular orbital (LUMO). When the silver electrode device is irradiated, photons from sunlight pass through the glass and ITO and are absorbed by CuPc, where excitons are created. Some of these excitons diffuse to the CuPc-Ag interface where, following an energy exchange, electron-hole pairs are created. Due to the built-in electric field at the interface, the light-generated holes then move into CuPc and are ultimately collected at the ITO electrode. This constitutes a current $I_{LIGHT} = I_L$, which, in the presence of a finite external load, makes ITO positively charged with respect to the silver electrode, thus forward biasing the Schottky diode by V_F. The forward bias causes an injection of holes from ITO to CuPc and of electrons from aluminum to CuPc, resulting in a loss current I_F in a direction opposite to I_L. The difference (I_L-I_F) is the current supplied by the solar cell to the load. When the load is

infinite (open-circuit), I_L-I_F = 0 and V_F = V_{oc} = open-circuit voltage. Clearly, V_{oc} cannot exceed V_{bi} where V_{bi} = $Ø_S$-$Ø_M$; where $Ø_S$ and $Ø_M$ are work functions of the CuPc semiconductor and the metal layer, respectively. V_{bi} values from Figures 5.1-5.4 are 1.19, 0.99, 0.77 and 0.15 V, respectively. Corresponding V_{oc} values from experimental data for Al, Cu, Ag and Au electrodes, as seen in Figure 4.22, are 1.15, 0.37, 0.25 and 0.12 V, respectively. Since the V_{bi} value for aluminum is the highest, one might expect its V_{oc} value to be the highest as well, which is indeed the case. However, since the work functions of aluminum [29] and silver [30] are not very far apart (4.06 and 4.26 eV, respectively), the observed large difference in their open circuit voltages is unexpected. We attribute this low V_{oc} in the case of silver to, (i) surface damage and creation of states in the energy gap of the underlying PTCBI and CuPc layers and, (ii) chemical reactivity or diffusion into the organic semiconductor layers during the deposition of silver. For the aluminum electrode case, on the other hand, it is proposed that a thin protective interlayer of aluminum oxide forms between aluminum and PTCBI during the electrode deposition. This hypothesis is motivated by the well-known fact that aluminum is a getter material for oxygen and will easily form an oxide when the vacuum level is not extremely high. This oxide layer protects the underlying PTCBI and CuPc films from damage and chemical reactivity. Of course, the presence of a highly resistive Al_2O_3 interlayer would lead to a higher series resistance, a lower fill factor and a reduction in J_{sc} in the solar cell; which is indeed observed in our experiments. Similarly, low values of V_{oc} for Au and Cu electrodes can be partially attributed to the damage to the surface and diffusion into underlying organic semiconductor layers. As the metallic electrode is deposited, diffusion into the underlying PTCBI and CuPc layers would reduce their effective thicknesses. It should be noted that PTCBI is only 7 nm thick and gold

is a relatively heavy atom; atomic weights of Au, Ag, Cu and Al are 197, 108, 68 and 27, respectively. Shunt resistances and V_{oc} values are in the reverse order with respect to the atomic weight values. In summary, when aluminum was used as an electrode, a high V_{oc} of 1.15V was observed. We attribute this high V_{oc} to, (i) reduced surface states formation due to damage from aluminum deposition, (ii) reduced electrode diffusion and therefore less reduction in effective thickness of organic semiconductor layer and, (iii) reduced tunneling losses across the junction. These advantages are thought to be enabled by the formation of a thin aluminum oxide interlayer between the aluminum electrode and CuPc during the Al deposition. High V_{oc} values were not achieved with Ag, Cu and Au electrodes because of the absence of this thin insulating oxide interlayer. On the other hand, electrons must tunnel across the aluminum oxide interlayer and this adds to the effective series resistance of the device. Thus, the fill factor and J_{sc} are reduced in the case of aluminum electrode. If a method for controlling the thickness of the insulating oxide layer could be found, then it may be possible to achieve a high V_{oc} as well as a high J_{sc} in these cells. When the thickness of PTCBI is large (greater than 15 nm), the dominant junction is the heterojunction between modified-CuPc and PTCBI instead of a Schottky diode between CuPc and the metal electrode. Energy level diagrams for CuPc/PTCBI/Al and CuPc/ PTCBI/Ag device structures are sketched in Figure 5.5 and 5.7 respectively. Comparing Figure 5.5 and 5.7 we see that the value of V_{bi} is 1.04 eV for the heterojunction case compared to 1.19 eV for the Schottky diode case. Therefore, a reduced V_{oc} can be expected for the heterojunction, which is observed. Furthermore, as the PTCBI layer is made thicker, excitons have to travel farther and recombination losses increase, resulting in yet lower J_{sc} and V_{oc}. This is seen in the data of Figure 4.11. And once the heterojunction becomes the dominant junction, the

aluminum electrode has no advantage over the silver electrode. In fact, higher J_{sc} is achieved in the device with silver electrode because the aluminum oxide layer is absent. Still, the V_{oc} value for the silver device is substantially smaller than the V_{bi} value of 0.95 V at the heterojunction. This indicates that, in spite of ‘‘thicker’’ PTCBI layer, there may still be some damage to the CuPc-PTCBI junction during the deposition of silver electrode. This issue necessitates further research. As for the addition of a thin CdS layer to the device configuration of Figure 3.1, it is thought that CdS, being more conductive than PTCBI, makes a better conducting contact to Al. It is advantageous, therefore, to insert a CdS layer between PTCBI and Al. On the other hand, PTCBI seems to modify the CuPc surface and make it more conductive. This advantage is lost when CdS is inserted between CuPc and PTCBI.

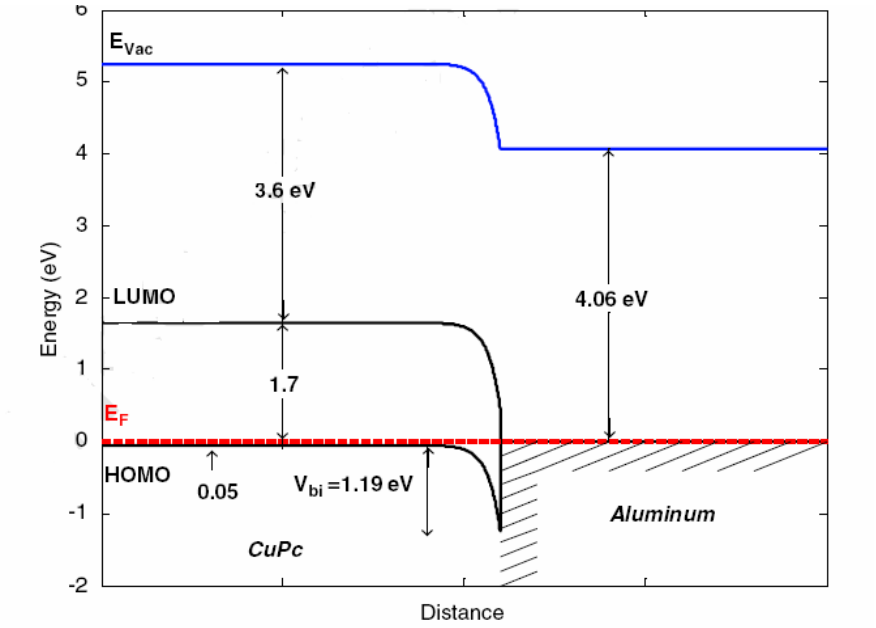

Figure 5.1: Energy level diagram of a CuPc-Al Schottky diode, in equilibrium.

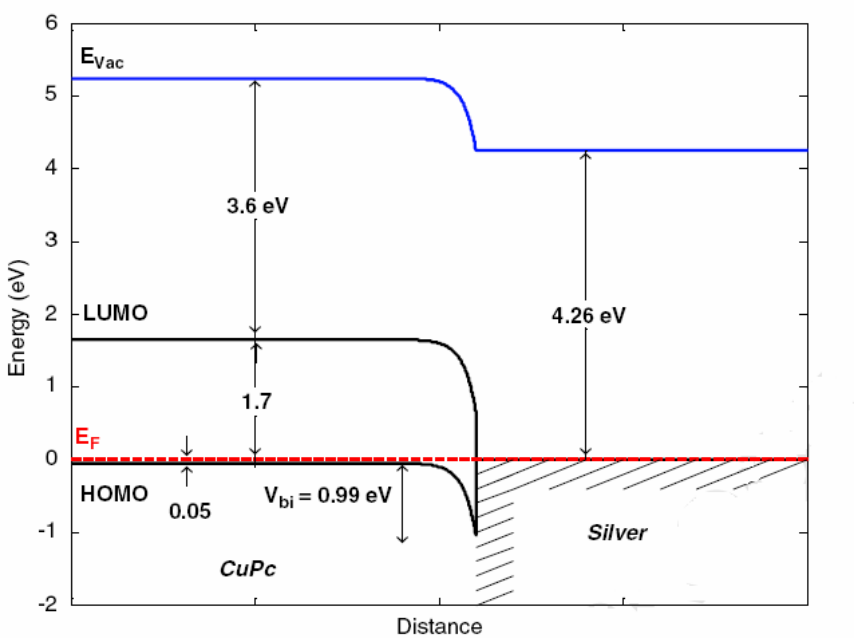

Figure 5.2: Energy level diagram of a CuPc-Ag Schottky diode, in equilibrium.

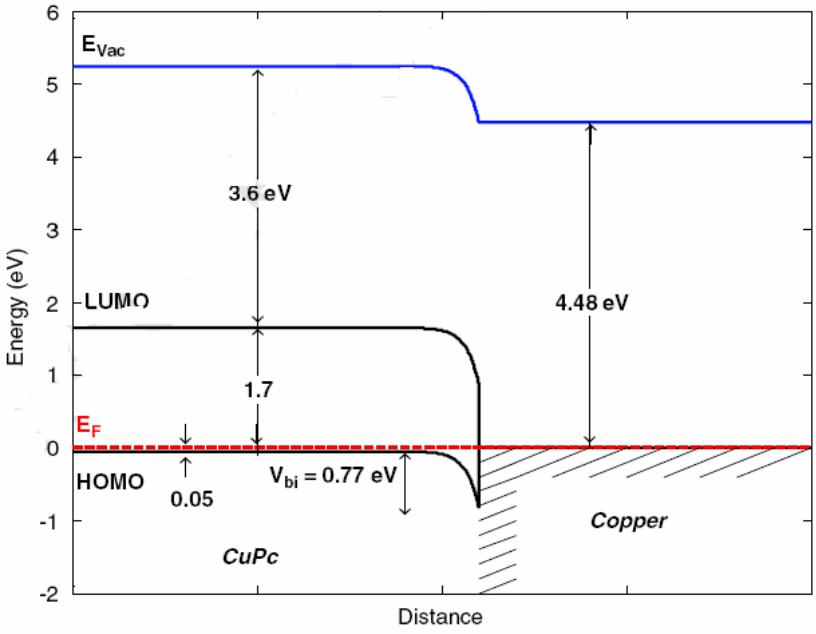

Figure 5.3: Energy level diagram of a CuPc-Cu Schottky diode, in equilibrium.

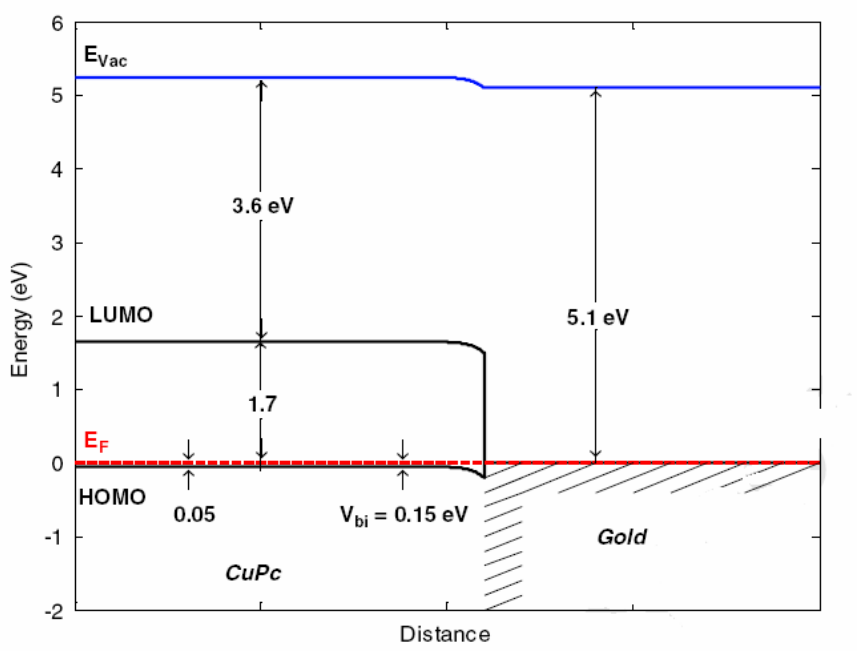

Figure 5.4: Energy level diagram of a CuPc-Au Schottky diode, in equilibrium.

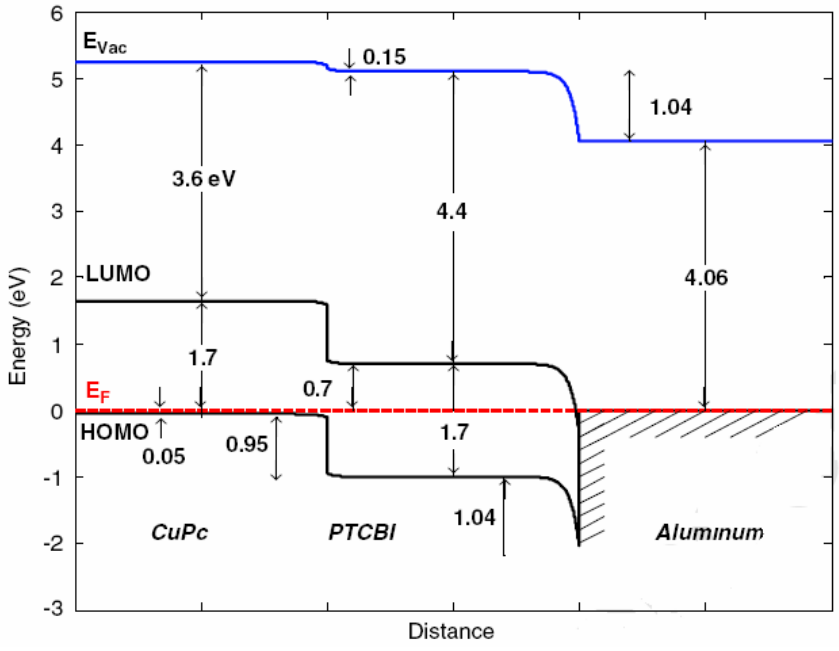

Figure 5.5: Energy level diagram of a CuPc-PTCBI-Al device, in equilibrium.

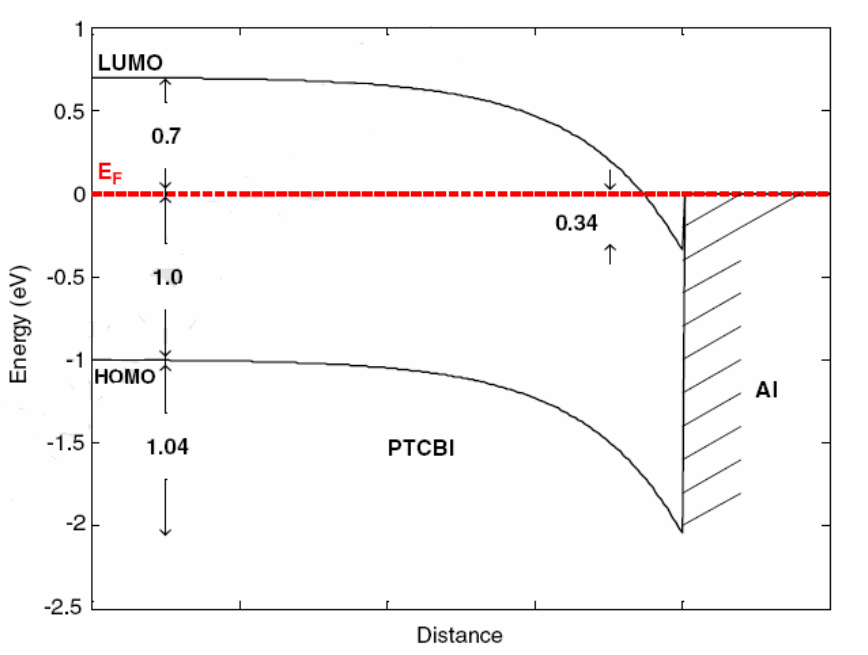

Figure 5.6: Detailed view of PTCBI-Al junction in a CuPc-PTCBI-Al device.

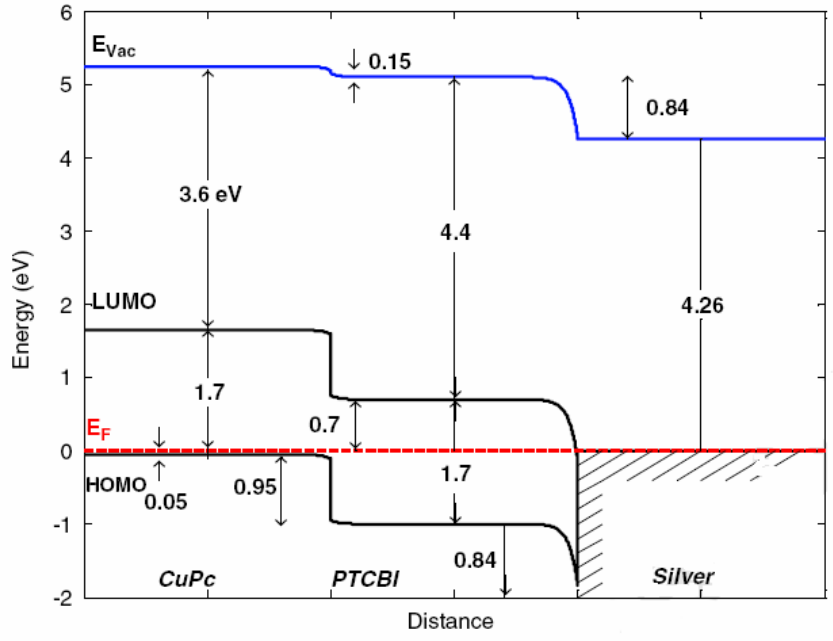

Figure 5.7: Energy level diagram of a CuPc-PTCBI-Ag device, in equilibrium.

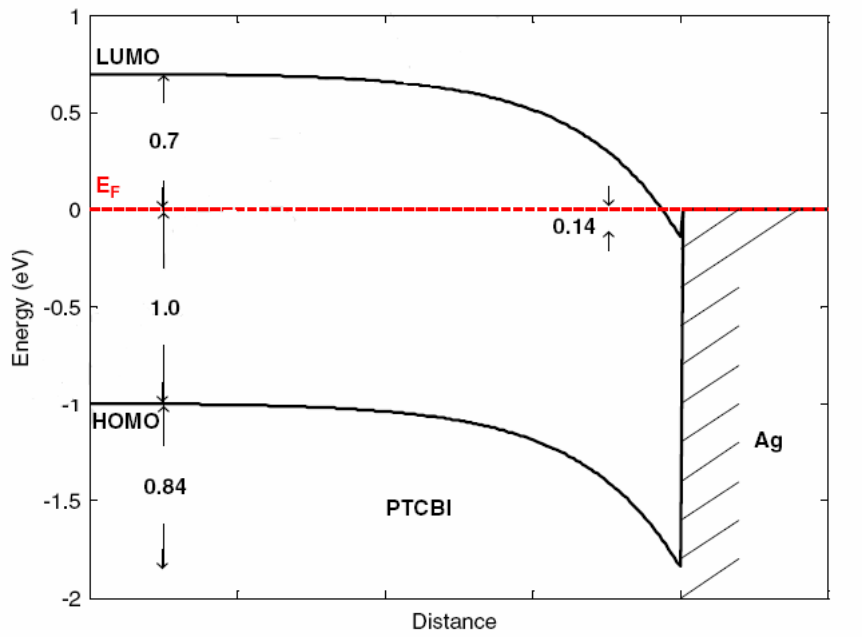

Figure 5.8: Detailed view of PTCBI-Ag junction in a CuPc-PTCBI-Ag device.

Chapter 6. Conclusion

In this work, solar cell structures involving CuPc, PTCBI were investigated. A high open circuit voltage of 1.15 V was obtained in an ITO/PEDOT:PSS/CuPc/PTCBI/Al device with a thin PTCBI layer of 7 nm thickness. Lower photovoltages were observed with thicker PTCBI layers and also with silver, copper and gold electrodes. Results were interpreted in terms of a modified CuPc-Al Schottky diode for the thin PTCBI case and a CuPc-PTCBI heterojunction for the thick PTCBI case. Also, the formation of a thin aluminum oxide layer under the aluminum electrode was postulated. This layer has a beneficial aspect in that shunting losses are reduced and a high photovoltage is enabled. However, it adds greatly to the series resistance to a point where the short-circuit current density is reduced. However, short-circuit current densities with silver, copper and gold electrodes were much higher than in the case of aluminum electrode (i.e. 4 mA/cm^2 vs. 0.12 mA/cm^2). From the current–voltage characteristics, it became clear that the devices with the Al electrode have a very different behavior than the devices with the other three electrodes. In the case of the latter devices, the characteristics follow a pattern that depends not only on their work functions but also on the damage done by these electrode materials to the underlying organic semiconductor layers during vacuum deposition. Experiments with the insertion of a thin LiF layer between PTCBI and the aluminum electrode showed no particular advantage indicating that this layer is not necessary in our devices. This thesis paves way to further work, that would involve a better understanding and control of the aluminum oxide layer and also experimentation using the various metal electrodes, with a view toward achieving high short-circuit current density.

References

1. C. W. Tang, Applied Physics Letters, Two-layer organic photovoltaic cell, Vol. 48, No. 183 (1986).

2. P. Peumans, A. Yakimov, and R. Forrest, Small molecular weight organic thin-film photodetectors and solar cells, Journal of Applied Physics, Vol. 93, No. 3693 (2003).

3. J. C. Scott, Metal-organic interface and charge injection in organic electronic devices, Journal of Vacuum Science & Technology A Vol. 21, No. 521 (2003).

4. J. Nelson, J. Kirkpatrick, and P. Ravirajan, Factors limiting the efficiency of molecular photovoltaic devices, Physical Review B Vol. 69, No. 035337 (2004).

5. V. P. Singh, O. M. Erickson, and J. N. Chao, Analysis of contact degradation at the CdTe-electrode interface in thin film CdTe-CdS solar cells, Journal of Applied Physics, Vol. 78, No. 4538 (1995).

6. N. J. Ekins-Daukes, K. W. J. Barnham, J. P. Connolly, J. S. Roberts, J. C. Clark, G. Hill, and M. Mazzer, Strain-balanced GaAsP/InGaAs quantum well solar cells, Applied Physics Letters, Vol. 75, No. 4195 (1999).

7. V. P. Singh, D. L. Linam, D. D. Dils, J. C. McClure, and G. B. Lush, Electro-optical characterization and modeling of thin film CdS-CdTe heterojunction solar cells, Solar Energy Materials and Solar Cells, Vol. 63, No. 445 (2000).

8. V. P. Singh, R. S. Singh, G. W. Thompson, V. Jayaraman, S. Sanagapalli, and V. K. Rangari, Characteristics of nanocrystalline CdS films fabricated by sonochemical, microwave and solution growth methods for solar cell applications, Solar Energy Materials and Solar Cells, Vol. 81, No. 293 (2004).

9. P. Peumans, V. Bulovic, and R. Forrest, Efficient photon harvesting at high optical intensities in ultrathin organic double-heterostructure photovoltaic diodes Applied Physics Letters, Vol. 76, No. 2650 (2000).

10. S. Barth and H. Baessler, Intrinsinc photoconduction in PPV-Type conjugated polymers, Physical Review Letters, Vol. 79, No. 4445 (1997).

11. P. G. d. Costa and E. M. Conwell, Excitons and the band gap in PPV, American Physical Society – Rapid Communications, Vol. 48, No. 1993 (1993).

12. R. N. Marks, J. J. Halls, D. D. C. Bradley, R. H. Friend and A. B. Holmes, The photovoltaic response in PPV thin film devices, Journal of Physics – Condensed Matter, Vol. 6, No. 1379 (1994).

13. Klaus Petritsch, Organic solar cell architectures, Ph. D Thesis (2000).

14. J. Nelson, Organic photovoltaic films, Solid State and Materials Science, Vol. 6, No. 87 (2002).

15. P. Peumans and S. R. Forrest, Very-high-efficiency double-heterostructure copper Phthalocyanine/C60 photovoltaic cells, Vol.79, No. 126 (2001).

16. C. J. Brabec, S. E. Shaheen, C. Winder, N. S. Sariciftci and P. Denk, Effect of LiF/metal electrodes on the performance of plastic solar cells, Vol. 80, No. 1288 (2002).

17. R. V. Stuart, Vacuum Technology, Thin Films and Sputtering, an Introduction, Academic Press, Inc. (1983).

18. C. Y. Kwong, A. B. Djurisic, P. C. Chui, L. S. M. Lam, and W. K. Chan, Improvement of the efficiency of Phthalocyanine organic Schottky solar cells with ITO electrode treatment, Applied Physics A, Material Science and Processing, Vol. 77, No. 555 (2003).

19. T. Aernouts, W. Geens, J. Poortmans, P. Heremans, S. Borghs, R. Mertens, Extraction of bulk and contact components of the series resistance in organic bulk donor-acceptor-heterojunctions, Thin Solid Films, Vol. 403, No. 297 (2002).

20. V. P. Singh, R. S. Singh, B. Parthasarathy, A. Aguilera, J. Anthony and M. Payne, Copper-phthalocyanine-based organic solar cells with high open-circuit voltage, Applied Physics Letters, Vol. 86, No 082106 (2005).

21. CRC Handbook of Chemistry and Physics, 74th Edition, CRS Press, No. 79-80 (1993).

22. S. M. Sze, Physics of Semiconductor Devices, 2nd Edition, Wiley Publications (2001).

23. P. Peumans, S. Vchida and S. R. Forrest, Efficient bulk heterojunction photovoltaic cells using small molecular weight organic thin films, Letters to nature, Vol. 425, No 158 (2003).

24. Wenping Hu and Michio Matsumura, Structure and thickness dependence of p-n heterojunction solar cells based on copper phthalocyanine and perylene pigments, Journal of Physics D Applied Physics, Vol. 37, No. 1434 (2004).

25. F. F. So, S. R. Forrest, Y. Q. Shi and W. H. Steier, Quasi-epitaxial growth of organic multiple quantum well structures by organic molecular beam deposition, Applied Physics Letters, Vol. 56, No. 674 (1990).

26. Jungyoon E, S. Kim, E. Lim, K. Lee, Effects of substrate temperature on copper(II) phthalocyanine thin films, Applied Surface Science, Vol. 205, No. 274 (2003).

27. C. Bobisch, Th. Wagner, A. Bannani, and R. Moller, Ordered binary monolayer composed of two organic moleculres: Copper Phthalocyanine and 3,4,9,10-perylene-tetra-carboxylic-dianhydride on Cu(111), Journal of Chemical Physics, Vol. 119, No. 9804 (2003).

28. Rudiono, F. Kaneko and M. Takeuchi, Morphological characteristics of perylene-doped phthalocyanine thin films and their photovoltaic effect, Applied Surface Science, Vol. 142. No. 598 (1999).

29. I. G. Hill, J. Schwartz and A. Kahn, Metal-dependent charge transfer and chemical interaction at interfaces between 3,4,9,10-perylenetetracarboxylic bismidazole and gold, silver and magnesium, Organic Electronics, Vol. 1, No. 5 (2000).

30. R. M. Eastment and C. H. B. Mee, Work function measurements on (100), (110) and (111) surfaces of aluminium, Journal of Physics F Metal Physics, Vol. 3, No. 1738 (1973).

Vita

Balaji Parthasarathy was born in Chennai, Tamil Nadu, India on April 19, 1979. He received his Bachelor of Engineering degree in Electrical and Electronics in April 2000 from the University of Madras. He worked as a Research Assistant from January 2003 – August 2004 in the Electronics Devices Research Group at the University of Kentucky, Lexington, Kentucky, USA. His journal publications are listed below.

1. Copper Phthalocyanine based organic solar cells with high open circuit voltage, Journal of Applied Physics Letters, 86, 082106 (2005), V. P. Singh, R. S. Singh, B. Parthasarathy, A. Aguilera, J. Anthony and M. Payne.
2. High photo voltage CuPc based organic solar cells, Journal of Solar Energy Materials and Solar Cells (in press), V. P. Singh, B. Parthasarathy, R. S. Singh, A. Aguilera, J. Anthony and M. Payne.